Fixed-Depth Two-Qubit Circuits and the Monodromy Polytope

Eric C. Peterson, Gavin E. Crooks, and Robert S. Smith
Rigetti Quantum Computing, 2919 Seventh St, Berkeley, CA 94710

For a native gate set which includes all single-qubit gates, we apply results from symplectic geometry to analyze the spaces of two-qubit programs accessible within a fixed number of gates. These techniques yield an explicit description of this subspace as a convex polytope, presented by a family of linear inequalities themselves accessible via a finite calculation. We completely describe this family of inequalities in a variety of familiar example cases, and as a consequence we highlight a certain member of the "XY–family" for which this subspace is particularly large, i.e., for which many two-qubit programs admit expression as low-depth circuits.

I. INTRODUCTION

Compilers for quantum computers have two primary tasks. One is to convert a hardware-agnostic description of an algorithm to a hardware-aware description suitable for execution on a particular physical device. This is an involved process, owing both to the idiosyncratic limitations of quantum computational devices and to the extremely large space of quantum programs. Ideal, "pure" quantum programs, which do not interact with the outside world until termination, can be interpreted as points in the projective unitary group $PU(2^q)$ (i.e., unitaries neglecting the effects of global phase), where q is the number of qubits in the system. For all positive values of q, $PU(2^q)$ is an infinite group, and so quantum compilers must draw on methods from continuous mathematics to accomplish their task. Optimized expression of a program, a compiler's second task, is of particular interest to programmers of quantum devices which do not yet enjoy fault tolerance. If each instruction has the potential to introduce error into the computation, then after sufficiently many instructions are enacted, the state of the quantum device will no longer even approximate the programmer's intent. Correspondingly, optimization passes in a quantum compiler which lower circuit depth provide a form of noise mitigation, and hence they contribute not just to expedience but to correctness.

In light of this observation, optimality results for decompositions are of interest to quantum compiler designers, and, in the presence of recursive or "trampolining" compilation schemes, such results for low numbers of qubits are particularly interesting. Some of the most advanced such results to date include: Shende, Bullock, and Markov [1] showed (using an earlier framework, see e.g. [2]) that all two-qubit programs can be expressed using three applications of the CZ–gate, interleaved with single-qubit rotations; Zhang, Vala, Sastry, and Whaley [3] showed that all two-qubit programs can be expressed using two applications of the B–gate, interleaved with single-qubit rotations; and the same group showed that a wide class of exponential families of two-qubit gates can be used to implement an arbitrary two-qubit program, using three applications interleaved with single-qubit rotations [4].

This first set of results has two particularly interesting features. First, the methods they describe are computationally tractable: one can actually construct their circuits by using standard algorithms in linear algebra. Second, they use the same techniques in a follow-up paper [5] to analyze the subspace of programs which take no more than two CNOTs to implement, and they conclude that "almost all" two-qubit programs take three invocations of CNOT to implement.

Although physical devices with native multi-qubit operations other than CNOT have been implemented, optimality results for these other native gate sets have not yet appeared. In this paper, we offer tools for the analysis of this problem, as well as fully worked examples for particularly interesting gate sets, at the following level of generality:

Theorem. *For S a finite set[1] of two-qubit operations and $n \geq 0$ a nonnegative integer, let P_S^n be the following set of two-qubit programs*

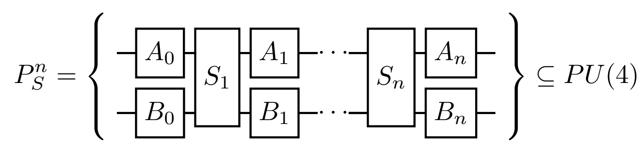

for $S_j \in S$ and $A_j, B_j \in PU(2)$.[2] In a certain coordinate system to be described below, P_S^n can be expressed a union of $(2|S|)^n$ convex polytopes, each described by a (typically highly redundant) family of linear inequalities of naive size exponential in n.

We use these results to explore the space of possible choices for the native gate set, with an emphasis on those appearing via Rigetti's choice of interaction Hamiltonian [6] (cf. also [7]): the gates CZ, iSWAP, CPHASE, and XY, where by XY we intend the unitary family

$$\mathrm{XY}_\theta = \exp\left(-\frac{1}{2} i\theta(\sigma_X^{\otimes 2} + \sigma_Y^{\otimes 2})\right)$$

---

[1] The finiteness assumption on S may be relaxed to account for such families as CPHASE_θ.

[2] Throughout, we write circuits right-to-left: the operator product AB is written in a circuit diagram as 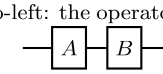 .

$$= \begin{pmatrix} 1 & 0 & 0 & 0 \\ 0 & \cos\left(\frac{\theta}{2}\right) & -i\sin\left(\frac{\theta}{2}\right) & 0 \\ 0 & -i\sin\left(\frac{\theta}{2}\right) & \cos\left(\frac{\theta}{2}\right) & 0 \\ 0 & 0 & 0 & 1 \end{pmatrix}.$$

Our methods in the case of $S = \{\mathrm{CZ}\}$ recover the results of Shende, Bullock, and Markov [1, 5]. In the other cases, we make the following conclusions:

Corollary. *The sets $P^2_{i\mathrm{SWAP}}$ and $P^3_{i\mathrm{SWAP}}$ are the same as the corresponding sets for $S = \{\mathrm{CZ}\}$. Hence, $P^2_{i\mathrm{SWAP}}$ has zero volume as a subset of all two-qubit programs.*

Corollary. *Allowing the parameter of* CPHASE *to range freely in $0 \le \theta \le 2\pi$, the sets P^2_{CPHASE} and P^3_{CPHASE} are the same as the corresponding sets for $S = \{\mathrm{CZ}\}$. Hence , P^2_{CPHASE} has zero volume as a subset of all two-qubit programs.*

We find the situation to be quite different for XY:

Corollary (Somewhat informal)**.** *As a function of θ, the volume of the set $P^2_{\mathrm{XY}_\theta}$ is maximized at $\theta = 3\pi/4$, where it contains 75% of the total volume of two-qubit programs. Allowing the parameter of* XY *to range freely, the set P^2_{XY} contains ≈96% of the total volume of all two-qubit programs.*

This has a number of interesting consequences: the most obvious is that the availability of gates in the XY family can have a dramatic effect on the optimal gate depth of a generic two-qubit program; another is that the bulk of this effect is seen by tuning up a *single* gate from this family. At the magic value of $\theta = 3\pi/4$, we provide an explicit routine for checking membership in this preferred subspace.

Our methods also lend themselves to an analysis of problems in approximate compilation. Each of the sets P^2_S described above is a proper subset of the space of all two-qubit programs, and for a two-qubit program G it is natural to search for "closest" two-qubit program to G within P^2_S is and to give a precise expression for this distance. We give a protocol describing the use of our techniques in this situation, and we give explicit computations of the best approximant and its minimum distance for certain interesting gates (e.g., SWAP) and interesting gate sets (e.g., $\mathrm{XY}_{\frac{3\pi}{4}}$).

We include as appendices an introduction to the mathematics underpinning these results as well as a simpler viewpoint that yields similar qualitative results but is quantitatively inexplicit.

II. THE GEOMETRY OF TWO-QUBIT PROGRAMS AND THE CANONICAL DECOMPOSITION

As motivation, we include a brief treatment of the Euler decomposition of single-qubit programs into triples of rotations. We begin by fixing notation:

$$\mathrm{X}_\alpha = \begin{pmatrix} \cos\frac{\alpha}{2} & -i\sin\frac{\alpha}{2} \\ -i\sin\frac{\alpha}{2} & \cos\frac{\alpha}{2} \end{pmatrix}, \quad \mathrm{Y}_\alpha = \begin{pmatrix} \cos\frac{\alpha}{2} & -\sin\frac{\alpha}{2} \\ \sin\frac{\alpha}{2} & \cos\frac{\alpha}{2} \end{pmatrix},$$

$$\mathrm{Z}_\alpha = \begin{pmatrix} e^{-i\frac{\alpha}{2}} & 0 \\ 0 & e^{i\frac{\alpha}{2}} \end{pmatrix}.$$

Theorem 1 (YZY–Euler decomposition, [8, pg. 189–207])**.** *Any single-qubit program $U \in PU(2)$ can be expressed as a triple of rotations:*

$$U = \mathrm{Y}_\alpha \cdot \mathrm{Z}_\beta \cdot \mathrm{Y}_\gamma,$$

where $0 \le \beta \le \pi$.[3]

Proof. We make use of the involution $\theta(U) = U^T$, referred to as a *Cartan involution*. The function θ is nontrivial in the sense that it admits a pair of exponential families Y_α and Z_β satisfying [4]

$$\theta(\mathrm{Y}_\alpha) = \mathrm{Y}_{-\alpha}, \qquad \theta(\mathrm{Z}_\beta) = \mathrm{Z}_\beta.$$

Inspired by the product form that we are pursuing, we consider the *Cartan double* of U:

$$\gamma(U) = U \cdot \theta(U) = UU^T.$$

In terms of the putative decomposition, this operation gives

$$\gamma(\mathrm{Y}_\alpha \cdot \mathrm{Z}_\beta \cdot \mathrm{Y}_\gamma) = \mathrm{Y}_\alpha \cdot \mathrm{Z}_{2\beta} \cdot \mathrm{Y}_{-\alpha}.$$

Indeed, UU^T is a symmetric unitary matrix, hence admits a basis of real eigenvectors. These can be used to determine the value of α; the eigenvalues of $\gamma(U)$ can be used to determine the value of 2β (and hence β); and, finally, the value of γ can then be determined from $\mathrm{Y}_\gamma = \mathrm{Z}_{-\beta} \cdot \mathrm{Y}_\alpha \cdot U$. □

Remark 2. This decomposition theorem gives rise to a wide family of other decompositions: any nonzero Lie algebra element $h \in \mathfrak{pu}(2)$ satisfying $\exp(2\pi \cdot h) = 1$ forms a maximal torus $H(t) = \exp(th)$ (which includes $\mathrm{Y}_t = \exp(-\frac{it}{2}\sigma_Y)$ and $\mathrm{Z}_t = \exp(-\frac{it}{2}\sigma_Z)$), and as any two maximal tori are conjugate in a compact Lie group, we may conjugate either one of the rolls appearing in Theorem 1 into a roll along our preferred axis, with the other coming along for the ride.

Remark 3. In the practice of microwave-driven superconducting qubits, there is some preferred roll—say, Z—which is a "virtual" operation, implemented as a frame shift, and hence is both instantaneous and immune to device error. Because of this, it is very common to conjugate the above decomposition by $Q = \mathrm{X}_{\frac{\pi}{2}}$ to instead produce a "ZYZ" version of the Euler decomposition.

[3] Moreover, for $0 < \beta < \pi$, the values $0 \le \alpha, \gamma \le 2\pi$ are essentially unique.

[4] This is most naturally expressed as a condition on the Lie algebra: the eigenspaces of $D\theta$ of weights 1 and -1 are both positive-dimensional.

We now turn to the analogous structure theorem for two-qubit operators:

Theorem 4 (“Canonical decomposition”, [2, Section III], [9, Theorem 2], [3, Section III.A.1]). *Any two-qubit unitary operator G admits an expression as*

$G =$ 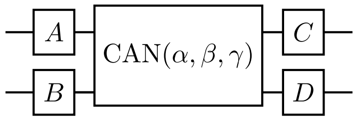 ,

where A, B, C, and D are single-qubit operators, where $\pi/4 \geq \alpha \geq \beta \geq |\gamma|$ are certain parameters, and where

$$\mathrm{CAN}(\alpha, \beta, \gamma) = \exp\left(\frac{-i}{2}(\alpha\sigma_x^{\otimes 2} + \beta\sigma_y^{\otimes 2} + \gamma\sigma_z^{\otimes 2})\right).$$

The parameter values are unique, and for generic parameter values the local gates are also unique.

Proof. As before, the Cartan involution $\theta(U) = U^T$ and associated Cartan doubling $\gamma(U) = UU^T$ give a decomposition of U into a product $O_L D O_R$, where these factors satisfy

$$O_L^T = O_L^{-1}, \qquad O_R^T = O_R^{-1}, \qquad D^T = D,$$

hence O_L and O_R are orthogonal matrices and D is a diagonal matrix. As with the translation from YZY–Euler decomposition to ZYZ–Euler decomposition, the theorem as stated arises by conjugating this decomposition by a particular operator Q,

$$Q = \frac{1}{\sqrt{2}}\begin{pmatrix} 1 & 0 & 0 & i \\ 0 & i & 1 & 0 \\ 0 & i & -1 & 0 \\ 1 & 0 & 0 & -i \end{pmatrix},$$

which satisfies $Q^\dagger PU(2)^{\otimes 2} Q = PO(4)$.[5,6] The gate family $\mathrm{CAN}(\alpha, \beta, \gamma)$ is then the conjugate of the diagonal matrices by Q. □

Remark 5. As in the single-qubit case, this decomposition is algorithmically effective: given a two-qubit gate G, by selecting angle values α, β, and γ the operator spectrum of $\gamma(G^Q)$ can be made to agree with that of $\mathrm{CAN}(\alpha, \beta, \gamma)$; a special-orthogonal matrix diagonalizing $\gamma(Q^\dagger G Q)$ recovers A and B; and, from this, one can then solve for C and D [5, Proposition IV.3]. The keystone of Shende, Bullock, and Markov is a process for manufacturing circuits with low CNOT–count for realizing particular values of $\mathrm{CAN}(\alpha, \beta, \gamma)$. In general, they show that this requires three applications of CNOT, and they moreover show which gates are accessible within two applications of CNOTs (cf. Appendix B): these are those gates whose canonical parameter γ is fixed at zero.

[5] Identifying a useful analogue of Q and of $PU(2)^{\otimes 2}$ is the primary inhibitor of generalizing this to higher qubit counts.

[6] See [5, Proposition IV.3] for a list of references concerning the provenance of this operator Q.

Remark 6. Also as in the case of ZYZ–Euler decomposition, this decomposition is arranged so that the outer factors have superior execution properties on many quantum devices. The outer factors are made up entirely of single qubit operators, which typically experience device errors at a rate 1–2 orders of magnitude less than multi-qubit operators, which must be used to express the middle factor. This prompts us to focus on the “hard” part of the problem—i.e., the middle factor—and to consider the maximal torus of canonical gates as the “interesting” or “difficult” part of two-qubit program compilation.

III. THE MULTIPLICATIVE EIGENVALUE PROBLEM AND THE MONODROMY POLYTOPE

Shende, Bullock, and Markov’s description of those two-qubit programs accessible within two applications of CNOT relies on specific commutation relations and explicit computation (again, cf. Appendix B). We would like to ask a more general version of this same question:

Problem 7. Let E and F be fixed two-qubit gates.

1. Give a description of the subspace

   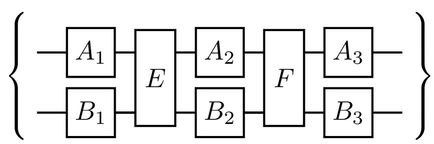 $\subseteq PU(4)$,

   for A_1, A_2, A_3, B_1, B_2, $B_3 \in PU(2)$.

2. Given $G \in PU(4)$ which is known to belong to this subset, algorithmically produce local gates A_1, A_2, A_3, B_1, B_2, and B_3 realizing G.

In this section, we show that this reduces to a well-known problem in representation theory, the *multiplicative eigenvalue problem*, whose solution comes in the form of the *monodromy polytope*.

For any such G, we apply the transformation

$$(-)^Q := Q^\dagger(-)Q$$

to produce $G^Q = O_1 E^Q O_2 F^Q O_3$, where O_1, O_2, O_3 are the orthogonal matrices conjugate to the indicated local gates under Q. In turn, E^Q and F^Q have orthogonal decompositions:

$$E^Q = O_{E,L} D_E O_{E,R}, \qquad F^Q = O_{F,L} D_F O_{F,R},$$

where D_E and D_F are diagonal and $O_{E,L}$, $O_{E,R}$, $O_{F,L}$, and $O_{F,R}$ are all orthogonal. Combining these decompositions yields

$$G^Q = O_1 O_{E,L} D_E O_{E,R} O_2 O_{F,L} D_F O_{F,R} O_3.$$

In order to place G^Q within the space of two-qubit gates, we then calculate its canonical parameters, which is equivalent to computing the spectrum of the Cartan double $\gamma(G^Q)$:

$$\begin{aligned}\gamma(G^Q) &= O_1 O_{E,L} D_E O_{E,R} O_2 O_{F,L} D_F O_{F,R} O_3 \cdot \\ &\quad (O_1 O_{E,L} D_E O_{E,R} O_2 O_{F,L} D_F O_{F,R} O_3)^T \\ &= O_1 O_{E,L} D_E O_{E,R} O_2 O_{F,L} D_F^2 \cdot \\ &\quad O_{F,L}^T O_2^T O_{E,R}^T D_E O_{E,L}^T O_1^T \\ &\sim O D_E^2 O^T D_F^2,\end{aligned}$$

where $O = O_{E,R} O_2 O_{F,L}$ is orthogonal and $\sim$ denotes unitary similarity. We have therefore reduced Problem 7 to the following:

Problem 8. Let D_E and D_F be fixed diagonal special unitary matrices.

1. Calculate the possible spectra of operators of the form $O D_E^2 O^T D_F^2$ as O ranges over orthogonal matrices.
2. Given a particular such operator spectrum D_G, calculate an orthogonal matrix O such that $O D_E^2 O^T D_F^2$ diagonalizes to give D_G^2.

Problem 8 is a restricted instance of the multiplicative eigenvalue problem:

Problem 9. Let U_1, U_2, and U_3 be unitary operators.

1. *Multiplicative eigenvalue problem*: Describe the possible spectra of all triples U_1, U_2, U_3 satisfying $U_1 U_2 U_3 = 1$ [7].
2. *Effective saturation problem*: Given a triple of operator spectra satisfying the conditions of (1), algorithmically produce U_1, U_2, and U_3 realizing these spectra and satisfying $U_1 U_2 U_3 = 1$.

What is immediately clear is that the collection of spectral quadruples satisfying Problem 8.1 can be converted to satisfy Problem 9.1. Continuing from the similarity relation above, the corresponding equation

$$\begin{aligned}O_{G,L} D_G^2 O_{G,L}^T &\sim O D_E^2 O^T D_F^2 \\ U^\dagger D_G^2 U &= O D_E^2 O^T D_F^2\end{aligned}$$

can be rewritten as

$$\begin{aligned}1 &= (O D_E^2 O^T) D_F^2 (U^\dagger (D_G^2)^\dagger U) \\ &= U_1 U_2 U_3,\end{aligned}$$

which shows that the spectra of D_E^2 and D_F^2 agree with those of U_1 and U_2, and the spectrum of D_G^2 agrees with that of $U_3^\dagger$. What is nonobvious is that the reverse inclusion is also true, which rests on a nontrivial result in symplectic geometry:

Theorem 10 ([10, Theorem 3])**.** *Let U_1, U_2, U_3 be a string of unitary operators satisfying $U_1 U_2 U_3 = 1$. Then there exist operators $V_1 \sim U_1$, $V_2 \sim U_2$, $V_3 \sim U_3$ within the unitary similarity classes of the originals which satisfy $V_1 V_2 V_3 = 1$ and for which V_1 and V_2 are simultaneously unitarily conjugate to symmetric unitaries, i.e., there exists a unitary W so that conjugating by W yields*

$$\begin{aligned}(W^\dagger V_1 W)(W^\dagger V_2 W)(W^\dagger V_3 W) &= 1 \\ (O_1^T D_1 O_1)(O_2^T D_2 O_2)(V_3') &= 1\end{aligned}$$

for some orthogonal matrices O_1, O_2 and diagonal matrices D_1, D_2 in the similarity classes of U_1, U_2. □

Corollary 11. *For U_1, U_2, and U_3 unitaries satisfying $U_1 U_2 U_3 = 1$ and with diagonalizations D_E^2, D_F^2, and $(D_G^2)^\dagger$ respectively, there exists an orthogonal matrix O and a unitary matrix U such that*

$$U^\dagger D_G^2 U = O D_E^2 O^T D_F^2,$$

i.e., solutions to Problem 9 give rise to solutions to Problem 8.

Proof. Start by applying the Theorem:

$$\begin{aligned}1 &= V_1 V_2 V_3 \\ &= (O_1^T D_E O_1)(O_2^T D_F O_2) W^\dagger V_3 W \\ O_2 W^\dagger V_3^\dagger W O_2^T &= O_2 O_1^T D_E^2 O_1 O_2^T D_F^2 \\ U^\dagger D_G^2 U &= O D_E^2 O^T D_F^2,\end{aligned}$$

where we have written $O = O_2 O_1^T$ and $U = E W O_2^T$ for E a matrix with columns an eigenbasis of $V_3^\dagger$. □

We now seek to enunciate the solution to Problem 9 given by Agnihotri, Meinrenken, and Woodward, which requires some supporting vocabulary. Primarily, there is a particular presentation of operator spectra which we will find useful:

Definition 12 (cf. [11, Chapter 4])**.** For a special unitary matrix U, we may uniquely present its spectrum

$$\operatorname{Spec} U = (e^{2\pi i \alpha_1}, \ldots, e^{2\pi i \alpha_n})$$

as

$$\operatorname{LogSpec} U = (\alpha_1, \ldots, \alpha_n),$$

where

$$\alpha_1 \leq \cdots \leq \alpha_n \leq \alpha_1 + 1, \qquad \alpha_+ := \sum_j \alpha_j = 0.$$

We refer to the collection of all such n–tuples as $\mathfrak{A}$, the *fundamental alcove* of $SU(n)$, and we will write $\operatorname{LogSpec} U$ for the associated point in $\mathfrak{A}$.

Let $C_2 \leq SU(n)$ be the finite central subgroup $\{\pm 1\}$, and let $U \in SU(n)/C_2$ be a member of the quotient group, which we may present as a coset

$$\{\tilde{U}, -\tilde{U}\} \subset SU(n).$$

[7] Of course, there is also a variant of the multiplicative eigenvalue problem concerning strings of operators of length $k \geq 3$.

The logarithmic spectra of these matrices

$$\alpha_* = \operatorname{LogSpec} \tilde{U}, \qquad \beta_* = \operatorname{LogSpec}(-\tilde{U})$$

are related by a form of rotation:

$$(\alpha_1, \alpha_2, \alpha_3, \alpha_4) = \rho\,(\beta_1, \beta_2, \beta_3, \beta_4) := \left(\beta_3 - \frac{1}{2}, \beta_4 - \frac{1}{2}, \beta_1 + \frac{1}{2}, \beta_2 + \frac{1}{2}\right).$$

By appropriately picking either $\operatorname{LogSpec} U = \operatorname{LogSpec} \tilde{U}$ or $\operatorname{LogSpec} -\tilde{U}$, we see that we may uniquely specify a sequence $\operatorname{LogSpec} U$ which further satisfies either

$$(\operatorname{LogSpec} U)_2 + 1/2 > (\operatorname{LogSpec} U)_4$$

or

$$\left\{ \begin{array}{c} (\operatorname{LogSpec} U)_2 + 1/2 = (\operatorname{LogSpec} U)_4 \\ \text{and} \\ (\operatorname{LogSpec} U)_1 + 1/2 \le (\operatorname{LogSpec} U)_3 \end{array} \right\},$$

where $(\operatorname{LogSpec} U)_j$ denotes the j^{th} component of the quadruple $\operatorname{LogSpec} U$. We similarly refer to the collection of all such n–tuples as $\mathfrak{A}_{C_2}$, the fundamental alcove of $SU(n)/C_2$.

Remark 13. The first variant is the natural target of the logarithmic spectrum of a special unitary operator, and it forms a convex polytope. This second variant is useful because it is the natural target of the logarithmic spectrum of the Cartan double of a *projective* unitary operator:

$$\operatorname{LogSpec} \gamma(-)\colon\ PU(4) \to \mathfrak{A}_{C_2}.$$

However, it does not quite form a convex polytope: the closure $\overline{\mathfrak{A}_{C_2}}$ is a convex polytope, but the values γ_* satisfying $\gamma_2 + 1/2 = \gamma_4$ and $\gamma_1 + 1/2 > \gamma_3$, which constitute half a face of $\overline{\mathfrak{A}_{C_2}}$, are missing from $\mathfrak{A}_{C_2}$.

Remark 14. The logarithmic spectrum γ_* of an operator U is related to its canonical coordinates as follows: starting with the triple

$$\left(\frac{\pi}{2} \cdot (\gamma_4 - \gamma_1), \frac{\pi}{2} \cdot (\gamma_3 - \gamma_1), \frac{\pi}{2} \cdot (\gamma_2 - \gamma_1)\right),$$

by applying permutations and the operators

$$(x, y, z) \mapsto (\pi - x, \pi - y, z)$$

there is a unique representative (x, y, z) satisfying $\pi/2 \ge x \ge y \ge |z|$. This triple gives the canonical coordinates of U.

Definition 15. The extremal points of the polytope $\overline{\mathfrak{A}_{C_2}}$ lie at the following coordinates:

$$\begin{aligned}
\operatorname{LogSpec} \gamma(I) &= e_1 = (0, 0, 0, 0), \\
\operatorname{LogSpec} \gamma(\mathrm{CZ}) &= e_2 = (-1/4, -1/4, 1/4, 1/4), \\
\operatorname{LogSpec} \gamma(i\mathrm{SWAP}) &= e_3 = (-1/2, 0, 0, 1/2), \\
\operatorname{LogSpec} \gamma(\mathrm{SWAP}) &= e_4 = (-3/4, 1/4, 1/4, 1/4), \\
\operatorname{LogSpec} \gamma(\sqrt{\mathrm{SWAP}}) &= e_5 = (-5/8, -1/8, 3/8, 3/8), \\
\rho \operatorname{LogSpec} \gamma(\sqrt{\mathrm{SWAP}}) &= e_6 = (-1/8, -1/8, -1/8, 3/8).
\end{aligned}$$

The subspace $\mathfrak{A}_{C_2}$ of $\overline{\mathfrak{A}_{C_2}}$ is given by deleting the subspace of convex combinations of e_2, e_3, and e_6 in which e_6 carries a nonzero coefficient.

We are now in a position to state the solution to Problem 9.1. We will give a more complete exposition of this result in Appendix A, but for our intended application we need only the following statement:

Theorem 16 (see Theorem 60)**.** *Let U_1, U_2, $U_3 \in SU(4)$ satisfy $U_1U_2 = (-1)^j U_3$ for some j (i.e., $U_1U_2 \equiv U_3$ as elements of $SU(4)/C_2$), and let*

$$\alpha_* = \operatorname{LogSpec} U_1, \quad \beta_* = \operatorname{LogSpec} U_2, \quad \gamma_* = \operatorname{LogSpec} U_3$$

be the associated logarithmic spectra. For $r, k > 0$ be positive integers with $r + k = n$, let $\mathcal{P}_{r,k}$ denote the set of partitions of k into r parts:

$$\mathcal{P}_{r,k} = \{(I_1, \ldots, I_r) \in \mathbb{Z}^r \mid 0 \le I_1 \le \cdots \le I_r \le k\}.$$

Select $r, k > 0$ satisfying $r + k = 4$, select $a, b, c \in \mathcal{P}_{r,k}$, and take $d \ge 0$; then if the associated quantum Littlewood–Richardson coefficient $N_{ab}^{c,d}(r, k)$ (see Definition 59 and Figure 10) satisfies $N_{ab}^{c,d}(r, k) = 1$, then the following inequality must hold:

$$d - \sum_{i=1}^{r} \alpha_{k+i-a_i} - \sum_{i=1}^{r} \beta_{k+i-b_i} + \sum_{i=1}^{r} (\rho^j \gamma)_{k+i-c_i} \ge 0. \quad (*)$$

The polytope defined by these inequalities is the monodromy polytope.

Moreover, given alcove sequences α_*, β_*, γ_* which belong to the monodromy polytope, then there must exist U_1, U_2, U_3 with

$$\alpha_* = \operatorname{LogSpec} U_1, \quad \beta_* = \operatorname{LogSpec} U_2, \quad \gamma_* = \operatorname{LogSpec} U_3$$

and which satisfy $U_1U_2 = (-1)^j U_3$ for some j. □

From this we draw the following consequence:

Corollary 17. *Let S be a gate set whose image through $\operatorname{LogSpec} \gamma(-)$ is a union of convex polytopes. The image of P_S^n through $\operatorname{LogSpec} \gamma(-)$ is then also a union of convex polytopes.*[8]

Proof. We have assumed the base case: $\operatorname{LogSpec} \gamma(P_S^1)$ is a union of convex polytopes. Assuming that $\operatorname{LogSpec} \gamma(P_S^{n-1})$ is a union of convex polytopes, each

[8] For gate sets S of interest to us, it is often the case that S appears as a subset of P_S^2. This condition entails the nesting property $P_S^n \subseteq P_S^{n+1}$ for $n \ge 2$.

constituent polytope is described by a finite collection of linear inequalities. The monodromy polytope is itself also described by a finite collection of linear inequalities. Select a polytope constituent of $\operatorname{LogSpec}\gamma(P^1_S)$ and of $\operatorname{LogSpec}\gamma(P^{n-1}_S)$. By imposing those linear inequalities describing the constituent of $\operatorname{LogSpec}\gamma(P^1_S)$ on the first coordinate, imposing those linear inequalities describing the constituent of $\operatorname{LogSpec}\gamma(P^{n-1}_S)$ on the second coordinate, and using Fourier–Motzkin elimination to project to the final coordinate, we produce a subset of $\operatorname{LogSpec}\gamma(P^n_S)$ which is described by a finite collection of linear inequalities. It follows that this too is a convex polytope, and the entire set $\operatorname{LogSpec}\gamma(P^n_S)$ is the union of the convex polytopes formed in this way. □

The reader is invited to explore the details of Theorem 16 as recited in Appendix A, but we include here a hands-on analysis of the analogous single-qubit case. Suppose that only some parameter values for Z–gates are in our native gate set, but we may freely choose the parameter in our Y–gates. In this context, we then seek to answer the following question: which circuits can be built through longer sequences of these gates?

We begin with a circuit of the form $U = \mathrm{Z}_\alpha \mathrm{Y}_\beta \mathrm{Z}_\gamma$ with α, γ fixed and β allowed to range. Using YZY–Euler decomposition, this can be equivalently written as $\mathrm{Y}_\delta \mathrm{Z}_\varepsilon \mathrm{Y}_\lambda$, and hence $\mathrm{Y}^\dagger_\delta U \mathrm{Y}^\dagger_\lambda = \mathrm{Z}_\varepsilon$ gives us access to Z_ε with ε potentially distinct from α and γ. Using the two decompositions of U, we can explicitly solve for ε:

$$\begin{aligned}\chi(U)(z) &= z^2 - \operatorname{tr}(U) z + 1 \\ &= z^2 - 2z\cos\frac{\beta}{2}\cos\frac{\alpha+\gamma}{2} + 1, \\ \chi(U)(z) &= z^2 - 2z\cos\frac{\varepsilon}{2} + 1,\end{aligned}$$

hence

$$\frac{\varepsilon}{2} = \cos^{-1}\left(\cos\frac{\beta}{2}\cos\frac{\alpha+\gamma}{2}\right).$$

The role of β is thus in some sense to modulate the interference of α and γ, and the resulting value ε satisfies a kind of inequality: the possible values of $\operatorname{LogSpec} U$ (suitably reinterpreted for use with $PU(2)$) form a subset of the ray connecting $\operatorname{LogSpec} Z_{\alpha+\gamma}$ and $\operatorname{LogSpec} 1 = (0,0)$ [9]. However, the dependence of ε on β is decidedly nonlinear [10].

We now connect Theorem 16 to this result. In Figure 1, we provide a table of quantum Littlewood–Richardson coefficients relevant for $PU(2)$. The mathematics behind Theorem 16 then gives the following:

[9] As a consequence of the bounds on the possible values of β, this segment does not always make it all the way to $(0,0)$.

[10] An amusing corollary is that the specific value $\alpha = \gamma = \pi/2$ is sufficient to generate all other Z–rotations after insertion of a Y–rotation.

r	k	a	b	c	d	$N^{c,d}_{ab}(r,k)$
1	1	(0)	(0)	(0)	0	1
		(1)	(0)	(1)	0	1
			(1)	(0)	1	1

FIG. 1. Structure constants in $qH^*\mathrm{Gr}(1,1)$. There is a further symmetry relation $N^{c,d}_{ab}(r,k) = N^{c,d}_{ba}(r,k)$.

Corollary 18. *Suppose that U_1, U_2, $U_3 \in SU(2)$ satisfy $U_1 U_2 = U_3$, and let*

$$\begin{aligned}-1/2 \le \alpha_1 \le \alpha_2 \le 1/2, \\ -1/2 \le \beta_1 \le \beta_2 \le 1/2, \\ -1/2 \le \gamma_1 \le \gamma_2 \le 1/2\end{aligned}$$

be the angles of their respective eigenvalues, expressed in revolutions. For a, b, c, d as listed in Figure 1, the following inequality must hold:

$$d - \alpha_{2-a} - \beta_{2-b} + \gamma_{2-c} \ge 0. \qquad (*)$$

Moreover, given values of α_*, β_*, γ_* satisfying these inequalities, there then exist U_1, U_2, U_3 which satisfy $U_1 U_2 = U_3$ as well as

$$\alpha_* = \operatorname{LogSpec} U_1, \qquad \beta_* = \operatorname{LogSpec} U_2,$$

$$\gamma_* = \operatorname{LogSpec} U_3.$$ □

Explicitly, these inequalities are

$$\begin{aligned}\alpha_1 + \beta_1 &\le \gamma_1, & \alpha_2 + \beta_1 &\le \gamma_2, \\ \alpha_2 + \beta_2 &\le \gamma_1 + 1, & \alpha_1 + \beta_2 &\le \gamma_2,\end{aligned}$$

or, in terms of $\alpha_2, \beta_2, \gamma_2 \ge 0$ alone,

$$\begin{aligned}-\alpha_2 + -\beta_2 &\le -\gamma_2, & \alpha_2 + -\beta_2 &\le \gamma_2, \\ \alpha_2 + \beta_2 &\le -\gamma_2 + 1, & -\alpha_2 + \beta_2 &\le \gamma_2,\end{aligned}$$

The resulting polytope is portrayed in Figure 2. Isolating γ_2 (or, equivalently, studying a vertical ray in the Figure above a particular choice of (α_2, β_2)), this yields

$$|\alpha_2 - \beta_2| \le \gamma_2 \le \min\{\alpha_2 + \beta_2, 1 - (\alpha_2 + \beta_2)\}.$$

A geometrical interpretation of this restriction is shown in Figure 3.

IV. MONODROMY POLYTOPE SLICES FOR THE STANDARD GATES

In this section, we consider the "standard gates" that appear in the paper of Smith, Curtis, and Zeng [12, Appendix A] and their effect as members of a native gate set. Each of these gates or gate families specify either a particular point in $\mathfrak{A}_{C_2}$ or a line segment in $\mathfrak{A}_{C_2}$, which

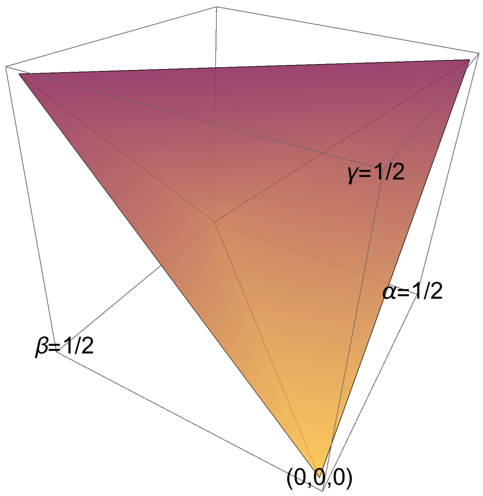

FIG. 2. Full monodromy polytope for $SU(2)$, shaded along the coordinate γ.

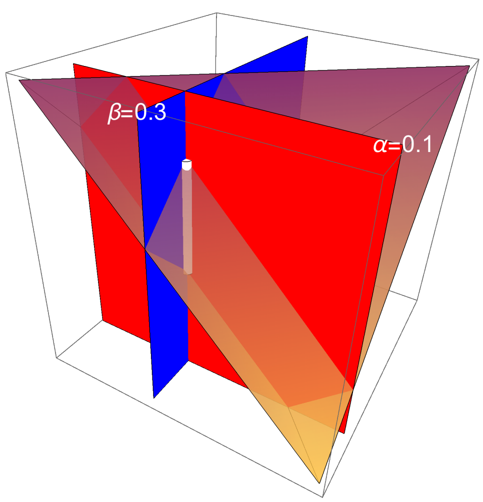

FIG. 3. The polytope intersected with the planes $\alpha = 0.1$, shaded red, and $\beta = 0.3$, shaded blue, resulting in restrictions on γ, shaded white.

in either case can be specified via a family of linear inequalities. By consequence, and similarly to the proof of Corollary 17, the space of programs which are accessible within a fixed number of applications of the native gates then appears as a projection of linear slice of the monodromy polytope. Our goal is to give descriptions of these projections.

A. The CZ gate

The sets $\operatorname{LogSpec} P^0_{\mathrm{CZ}}$ and $\operatorname{LogSpec} P^1_{\mathrm{CZ}}$ are singletons and hence automatically convex polytopes:

$$\operatorname{LogSpec} P^0_{\mathrm{CZ}} = e_1,$$
$$\operatorname{LogSpec} P^1_{\mathrm{CZ}} = e_2.$$

In order to compute $\operatorname{LogSpec} P^2_{\mathrm{CZ}}$, we intersect the polytope described in Theorem 16 with the six hyperplanes describing the conditions $\alpha_*, \beta_* \in \operatorname{LogSpec} P^1_{\mathrm{CZ}}$:

Lemma 19 (cf. [1, Proposition III.3])**.** $\operatorname{LogSpec} \gamma(P^2_{\mathrm{CZ}})$ *is the convex polytope described by*

$$\operatorname{LogSpec} \gamma(P^2_{\mathrm{CZ}}) = \left\{ (\gamma_1, \gamma_2, \gamma_3, \gamma_4) \in \mathfrak{A}_{C_2} \;\middle|\; \begin{array}{c} \gamma_1 = -\gamma_4, \\ \gamma_2 = -\gamma_3 \end{array} \right\}.$$

The extremal points of $\operatorname{LogSpec} \gamma(P^2_{\mathrm{CZ}})$ *are*

$\operatorname{LogSpec} \gamma \Big($ 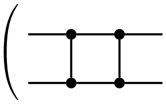 $\Big) = e_1,$

$\operatorname{LogSpec} \gamma \Big($ 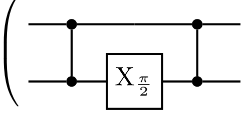 $\Big) = e_2,$

$\operatorname{LogSpec} \gamma \Big($ 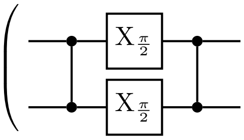 $\Big) = e_3.$

Proof. Using the quantum Littlewood–Richardson coefficients

$$N^{(2,0),0}_{(1,0)(1,0)}(2,2) = 1, \qquad N^{(1,1),0}_{(1,0)(1,0)}(2,2) = 1$$

we apply Theorem 16 to deduce the inequalities

$$\begin{aligned} 0 - (\alpha_{2+1-1} + \alpha_{2+2-0}) - (\beta_{2+1-1} + \beta_{2+2-0}) \\ + \gamma_{2+1-2} + \gamma_{2+2-0} \geq 0, \\ 0 - (\alpha_{2+1-1} + \alpha_{2+2-0}) - (\beta_{2+1-1} + \beta_{2+2-0}) \\ + \gamma_{2+1-1} + \gamma_{2+2-1} \geq 0, \end{aligned}$$

i.e.,

$$\begin{aligned} 0 - (1/4 + -1/4) - (1/4 + -1/4) + \gamma_1 + \gamma_4 \geq 0, \\ 0 - (1/4 + -1/4) - (1/4 + -1/4) + \gamma_2 + \gamma_3 \geq 0. \end{aligned}$$

Because of the additional constraint $\gamma_+ = 0$, we learn that these nonnegative quantities are in fact exactly zero:

$$\gamma_1 = -\gamma_4, \qquad \gamma_2 = -\gamma_3.$$

This plane passes through three of the extremal vertices of $\mathfrak{A}_{C_2}$, hence $\operatorname{LogSpec} \gamma(P^2_{\mathrm{CZ}})$ is contained inside of the triangle formed as the convex hull of those three vertices. In order to show that this inclusion is actually an equality, we need only produce witnesses that these three points have preimages in P^2_{CZ}. One checks that the circuits described above do the job: not only do they image to the appropriate vertex under $\operatorname{LogSpec} \gamma(-)$, but the mirroring value j in Theorem 16 is not used, so that these vertices belong to the same polytope. Hence, their convex hull is as claimed [11]. ☐

The briefest method for accessing P^3_{CZ} follows along identical lines: if we can show that the extremal vertices of $\mathfrak{A}_{C_2}$ have realizations within $\operatorname{LogSpec}\gamma(P^3_{\mathrm{CZ}})$ and we are allowed to apply convexity, then we can conclude the following equality [12]:

Lemma 20 (cf. [5, Section V])**.** $\operatorname{LogSpec}\gamma(P^3_{\mathrm{CZ}}) = \mathfrak{A}_{C_2}$, *where the following circuits realize the extremal points:*

$e_1 = \operatorname{LogSpec}\gamma\Bigg($ 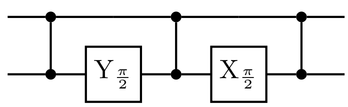 $\Bigg)$,

$e_2 = \operatorname{LogSpec}\gamma\Bigg($ 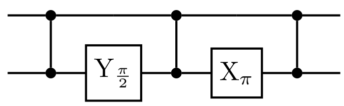 $\Bigg)$,

$e_3 = \operatorname{LogSpec}\gamma\Bigg($ 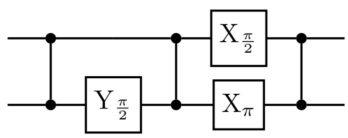 $\Bigg)$,

$e_4 = \operatorname{LogSpec}\gamma\Bigg($ 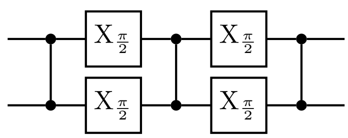 $\Bigg)$,

$e_5 = \operatorname{LogSpec}\gamma\Bigg($ 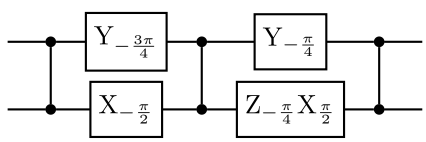 $\Bigg)$.

Proof. It is automatic that we have $\operatorname{LogSpec}\gamma(P^3_{\mathrm{CZ}}) \subseteq \mathfrak{A}_{C_2}$. In order to show the opposite inclusion, we need to supply the necessary realizations (with the necessary mirroring property, as in the proof of Lemma 19). One may check directly that the circuits above will do. ☐

Remark 21. In order to explain the provenance of the first three circuits in the Lemma statement, we remark that Lemma 19 shows that $\mathrm{CZ} \in P^2_{\mathrm{CZ}}$, and hence we are led to the method suggested by Corollary 17. Beginning with the realization of the extremal vertex $e_2 \in \operatorname{LogSpec}\gamma(P^2_{\mathrm{CZ}})$, we need only solve for the outer local gates to realize CZ exactly, as in:

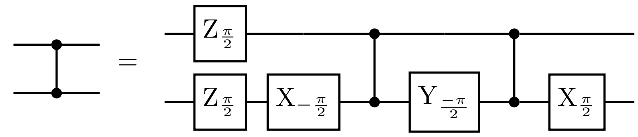

Using this formula, we may augment the other realizations of the extremal vertices of $\operatorname{LogSpec}\gamma(P^2_{\mathrm{CZ}})$ into realizations in $\operatorname{LogSpec}\gamma(P^3_{\mathrm{CZ}})$ by substituting the above circuit for CZ in for, say, the left-hand CZ supplied in Lemma 19. The realization supplied for the fourth extremal vertex is a rephrasing of the usual expression of SWAP as a triple of alternating CNOTs, and the fifth we produced by numerical search.

Remark 22 ([5, Proposition V.1])*.* Critically for quantum compilation, a circuit realization for any point within $\operatorname{LogSpec}\gamma(P^3_{\mathrm{CZ}})$ can be exactly produced algorithmically. The circuit proposed by Shende, Markov, and Bullock is

$\mathrm{CAN}(\alpha, \beta, \gamma) \equiv$ 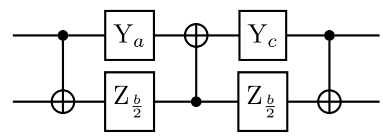 ,

where a, b, and c are certain linear functions of α, β, and γ. In general, exact decompositions do not seem to exist, and even numerical methods pose a challenge; see Section VII.

B. The *i*SWAP gate

Now we prove analogous results for $S = \{i\mathrm{SWAP}\}$. We will be briefer in the aspects that exactly mirror those for the gate CZ.

The sets $\operatorname{LogSpec}\gamma(P^0_{i\mathrm{SWAP}})$ and $\operatorname{LogSpec}\gamma(P^1_{i\mathrm{SWAP}})$ are again singletons:

$$\operatorname{LogSpec}\gamma(P^0_{i\mathrm{SWAP}}) = (0, 0, 0, 0),$$
$$\operatorname{LogSpec}\gamma(P^1_{i\mathrm{SWAP}}) = (-1/2, 0, 0, 1/2).$$

Lemma 23. $\operatorname{LogSpec}\gamma(P^2_{i\mathrm{SWAP}})$ *is described by*

$$\operatorname{LogSpec}\gamma(P^2_{i\mathrm{SWAP}}) = \left\{ \gamma_* \in \mathfrak{A}_{C_2} \;\middle|\; \begin{array}{l} \gamma_1 = -\gamma_4, \\ \gamma_2 = -\gamma_3 \end{array} \right\}.$$

The extremal points of $\operatorname{LogSpec}\gamma(P^2_{i\mathrm{SWAP}})$ *are*

$\operatorname{LogSpec}\gamma\Bigg($ 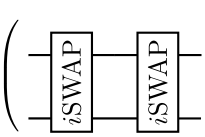 $\Bigg) = e_1,$

[11] One can avoid divine inspiration by instead producing the entire family of inequalities of Theorem 16, adding the equalities coming from our selection of $\alpha_* = \beta_* = \operatorname{LogSpec}\gamma(\mathrm{CZ})$, optionally pre-reducing the system, calculating all of the points of triple intersection, and throwing out those points which do not satisfy the original family of inequalities. This will, ultimately, produce the same set of extremal points. While this has the benefit of being mechanical (up to the point of calculating the realizations), it is quite arduous—and it does not produce the realizations of the extremal points as circuits.

[12] There is also the following alternative approach that mimics the alternative approach to P^2_{CZ}. By intersecting the full polytope described by Theorem 16 with the family of inequalities which constrain $\alpha_* \in \operatorname{LogSpec}\gamma(P^2_{\mathrm{CZ}})$ and with the equality which constrains $\beta_* = \operatorname{LogSpec}\gamma(\mathrm{CZ})$, we arrive at a convex polytope contained in $\mathfrak{A}_{C_2} \times * \times \mathfrak{A}_{C_2}$. Projecting to the last factor yields $\operatorname{LogSpec}\gamma(P^3_{\mathrm{CZ}})$, which we can accomplish by using Fourier–Motzkin elimination to delete the remaining degrees of freedom in the first factor. This, too, is completely mechanical but is even more arduous.

LogSpec γ (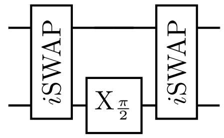) $= e_2$,

LogSpec γ (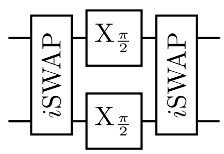) $= e_3$.

Proof. This proof entirely mimics that of Lemma 19, but this time the relevant quantum Littlewood–Richardson coefficients are

$$N^{(2,0),0}_{(0,0)(2,0)}(2,2) = 1, \qquad N^{(1,1),0}_{(1,0)(2,1)}(2,2) = 1. \qquad \square$$

Moving on to $P^3_{i\mathrm{SWAP}}$, we have

Lemma 24. $\mathrm{LogSpec}\,\gamma(P^3_{i\mathrm{SWAP}}) = \mathfrak{A}_{C_2}$, *with extremal realizations*

$e_1 =$ LogSpec γ (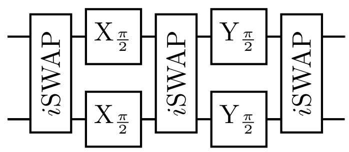),

$e_2 =$ LogSpec γ (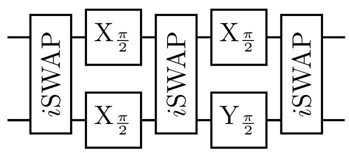),

$e_3 =$ LogSpec γ (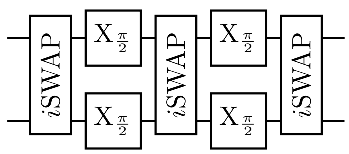),

$e_4 =$ LogSpec γ (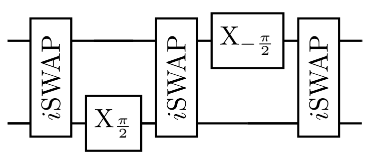),

$e_5 =$ LogSpec γ (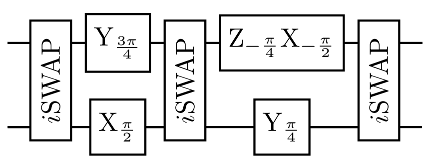).

Proof. Again, the proof is almost identical to that of Lemma 20, beginning with an exact realization of $i\mathrm{SWAP} \in P^2_{i\mathrm{SWAP}}$ by solving for the outer local gates in the realization of $e_3 = \mathrm{LogSpec}\,\gamma(i\mathrm{SWAP})$ in $\mathrm{LogSpec}\,\gamma(P^2_{i\mathrm{SWAP}})$:

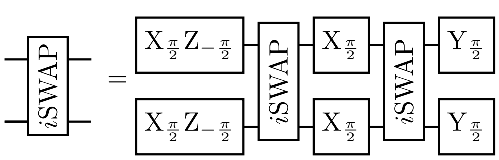

Using this, we can inflate the left-hand iSWAP in the realizations of the extremal vertices in Lemma 23 to produce realizations of those same vertices in $\mathrm{LogSpec}\,\gamma(P^3_{i\mathrm{SWAP}})$. What remains is to produce realizations of the extremal points SWAP and $\sqrt{\mathrm{SWAP}}$, where we rely on a standard decomposition. $\square$

Remark 25. Combining the results above with those from the previous subsection, we conclude

$$P^2_{\mathrm{CZ}} = P^2_{i\mathrm{SWAP}}, \qquad P^3_{\mathrm{CZ}} = P^3_{i\mathrm{SWAP}}.$$

As in the case of CZ, the compilation problem for iSWAP (i.e., Problem 7.2 and its depth-three variant) admits exact solutions. This does not appear to be in the literature, and so we include an analysis here:

Corollary 26. *For* $1/2 \geq \alpha \geq \beta \geq 0$, *the operator*

$U(\alpha, \beta) =$ 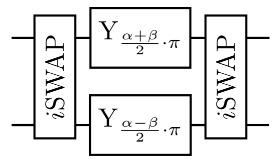

satisfies

$$\mathrm{LogSpec}\,\gamma(U(\alpha,\beta)) = (-\alpha, -\beta, \beta, \alpha).$$

Proof. After conjugation by $\mathrm{X}_{\frac{\pi}{2}} \otimes \mathrm{X}_{\frac{\pi}{2}}$, the operator $U(\alpha,\beta)$ expresses a pair of uniformly controlled rolls: a Z–roll by $\frac{\pm 1}{2}(\alpha - \beta)$ on the first qubit and a Z–roll by $\frac{\pm 1}{2}(\alpha + \beta)$ on the second. It follows that the eigenvalues of this operator are $(e^{i\alpha/2}, e^{-i\alpha/2}, e^{i\beta/2}, e^{-i\beta/2})$, and hence that the logarithmic spectrum of its Cartan double is as claimed. $\square$

Remark 27 (cf. [1, Proposition V.2]). Our strategy for algorithmically producing circuits for points in $P^3_{i\mathrm{SWAP}}$ will be to isolate the troublesome extremal vertex e_4. Once this vertex does not contribute to the remaining convex linear combination, the remainder is solved by Corollary 26. Selecting a gate $U \in PU(4)$, we seek local gates A and B so that

$V(U, A, B) :=$ 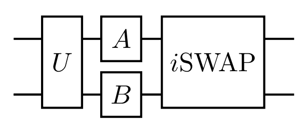

satisfies $\mathrm{LogSpec}\,\gamma(V(U,A,B)) \in P^2_{i\mathrm{SWAP}}$. We apply Lemma 23 to see that this is accomplished by finding values of A and B so that $\mathrm{tr}\,\gamma(V(p,A,B))$ is real. It will turn out that we may take $A = \mathrm{Y}_\sigma$ and $B = 1$, which we can see by manual calculation:

tr γ (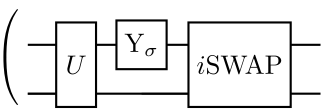)

$$= -2 \left(\sum_{j=1}^{4} u_{2j} u_{3(j+(-1)^j} - \sum_{k=1}^{4} u_{4k} u_{1(k+(-1)^k} \right) \cos\sigma$$

$$+ -2\left(\sum_{j=1}^{2}\sum_{k=1}^{4} u_{(2j)k}u_{(2j+1)(k-2)}(-1)^{(j-1)+k}\right)\sin\sigma,$$

where we have denoted the components of U according to

$$U = \begin{pmatrix} u_{11} & u_{12} & u_{13} & u_{14} \\ u_{21} & u_{22} & u_{23} & u_{24} \\ u_{31} & u_{32} & u_{33} & u_{34} \\ u_{41} & u_{42} & u_{43} & u_{44} \end{pmatrix},$$

and where we have interpreted the indices modulo 4. In particular, this summation formula enables us to solve the equation

$$\operatorname{Im}\left(\operatorname{tr}\gamma\left(V(U,\sigma)\right)\right) = 0$$

by picking a value of σ satisfying

$$\frac{-\operatorname{Im}\left(\sum_j u_{2j}u_{3(j+(-1)^j} - \sum_k u_{4k}u_{1(k+(-1)^k}\right)}{\operatorname{Im}\left(\sum_{j=1}^{2}\sum_k u_{(2j)k}u_{(2j+1)(k-2)}(-1)^{(j-1)+k}\right)} = \tan\sigma.$$

Because the tangent function is surjective, this equation is always soluble.

As one remaining case of interest, we can also describe the collection of gates accessible to a gate set that has *both* CZ and iSWAP available:

Lemma 28. *The set $P^2_{i\mathrm{SWAP,CZ}}$ is the union of $P^2_{i\mathrm{SWAP}}$, (or P^2_{CZ}) and the convex polytope*

$$\left\{\gamma_* = (\gamma_1,\gamma_2,\gamma_3,\gamma_4) \in \mathfrak{A}_{C_2} \,\middle|\, \begin{array}{c}\gamma_4 = 1/2 - \gamma_3, \\ \gamma_1 = -1/2 - \gamma_2\end{array}\right\},$$

which has extremal vertices e_2, e_3, e_4. □

This gate set also admits algorithmic decomposition, which one may verify by direct calculation:

Lemma 29. *For $\gamma_* \in \operatorname{LogSpec}\gamma(P^2_{i\mathrm{SWAP,CZ}})$, there are two entries satisfying*

$$-1/4 \le \gamma_i \le \gamma_j \le 1/4.$$

Setting $\alpha = (\gamma_i + \gamma_j)\pi$ and $\beta = (\gamma_i - \gamma_j)\pi$, we then have

$$\gamma_* = \operatorname{LogSpec}\gamma\left(\quad\right).$$

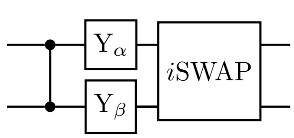

□

C. The CPHASE and PSWAP gate families

As further demonstration of these techniques, we also consider some combinations of the parametric two-qubit gates which appear in the Quil standard gate set [12].

Lemma 30. *The convex polytope* $\operatorname{LogSpec}\gamma(P^2_{\mathrm{CPHASE}})$ *agrees with* $\operatorname{LogSpec}\gamma(P^2_{\mathrm{CZ}})$ *and with* $\operatorname{LogSpec}\gamma(P^2_{i\mathrm{SWAP}})$.

Proof. The proof is identical to that given for Lemma 19: the same quantum Littlewood–Richardson coefficients impose the same symmetry relation on $\operatorname{LogSpec}\gamma(P^2_{\mathrm{CPHASE}})$, and the reverse inclusion then follows from $P^2_{\mathrm{CZ}} \subseteq P^2_{\mathrm{CPHASE}}$. □

Lemma 31. P^2_{PSWAP} *agrees with the other depth-two sets studied so far:*

$$P^2_{\mathrm{PSWAP}} = P^2_{\mathrm{CZ}} = P^2_{i\mathrm{SWAP}} = P^2_{\mathrm{CPHASE}}.$$

Proof. This proof proceeds similarly to that of Lemma 23. This time the relevant quantum Littlewood–Richardson coefficients are

$$N^{(2,0),1}_{(2,1)(2,1)}(2,2) = 1, \qquad N^{(1,1),1}_{(2,1)(2,1)}(2,2) = 1,$$

together with the calculation

$$\operatorname{LogSpec}\gamma(\mathrm{PSWAP}_\theta) = \left(-\frac{1}{4} - \frac{t}{2}, -\frac{1}{4} + \frac{t}{2}, -\frac{1}{4} + \frac{t}{2}, \frac{3}{4} - \frac{t}{2}\right).$$

An application of Theorem 16 yields inequalities which enforce the same symmetry conditions on $\operatorname{LogSpec}\gamma(P^2_{\mathrm{PSWAP}})$ as in the previous Lemmas. Because we have $P^2_{i\mathrm{SWAP}} \subseteq P^2_{\mathrm{PSWAP}}$, we may conclude equality. □

V. MONODROMY POLYTOPE SLICES FOR THE XY GATE FAMILY

Combining the ideas which motivated iSWAP and CPHASE, we are also motivated to consider the one-parameter family of native two-qubit gates given by

$$\mathrm{XY}_\theta = \exp\left(-\frac{i}{2}\cdot\theta\cdot(\sigma_x\sigma_x + \sigma_y\sigma_y)\right) = \begin{pmatrix} 1 & 0 & 0 & 0 \\ 0 & \cos(\theta/2) & -i\sin(\theta/2) & 0 \\ 0 & -i\sin(\theta/2) & \cos(\theta/2) & 0 \\ 0 & 0 & 0 & 1 \end{pmatrix}.$$

This family is interesting for a few reasons: it is one of the only remaining "edges" of $\mathfrak{A}$ (the other being a ray connecting I to SWAP); it can arise naturally as a gate natively available to systems where iSWAP is available, as in [6]; and it itself belongs to the canonical family.

Having noted that XY_θ belongs to the canonical family, we may compute its associated diagonal coordinates to be

$$\mathrm{XY}^Q_\theta = \begin{pmatrix} 1 & 0 & 0 & 0 \\ 0 & e^{i\theta/2} & 0 & 0 \\ 0 & 0 & e^{-i\theta/2} & 0 \\ 0 & 0 & 0 & 1 \end{pmatrix},$$

$$\operatorname{LogSpec}\gamma(\mathrm{XY}_\theta) = \left(-\frac{\theta}{2\pi}, 0, 0, \frac{\theta}{2\pi}\right).$$

In pursuit of an analogue of the results of Section IV C, we might perform an analysis of the polytope $\operatorname{LogSpec}\gamma(P^2_{\mathrm{XY}})$. However, the style of proof from Section IV C does not gain any traction: the intersection of the monodromy polytope with the hyperplanes

$$\alpha_* = (-s, 0, 0, s), \qquad \beta_* = (-t, 0, 0, t)$$

yields a rather complicated polytope in its wake, and applying Fourier–Motzkin elimination to the variables s and t does not appear to appreciably simplify the result. However, we can use this to efficiently test that particular points lie inside of $\operatorname{LogSpec}\gamma(P^2_{\mathrm{XY}})$, which includes the following nondegenerate set [13]:

$$\begin{aligned} &(0,0,0,0), && (-1/4,-1/4,1/4,1/4),\\ &(-1/2,0,0,1/2), && (-1/3,0,1/6,1/6). \end{aligned}$$

By consequence, $\operatorname{LogSpec}\gamma(P^2_{\mathrm{XY}})$ has nonzero volume—a stark difference from the situation of Section IV (and, in particular, of Section IV C).

Rather than pursue this complicated polytope directly, we first consider instead a simpler variant of the problem: given that the polytope $\operatorname{LogSpec}\gamma(P^2_{\mathrm{XY}})$ has positive volume, we can also ask whether any particular slice of it, given by fixing a particular value of θ, also contributes a nondegenerate subpolytope [14]. Just as the nondegeneracy of $\operatorname{LogSpec}\gamma(P^2_{\mathrm{XY}})$ is a surprising contrast to the results of Section IV C, the existence of such slices would be a surprising contrast to the results of Section IV A and Section IV B. Furthermore, if such slices do exist, we can ask an additional question: which particular values of θ maximize the volume of the slice?

Fix $0 \le \theta < \pi$, with corresponding value $t = \theta/(2\pi)$ satisfying $0 \le t < 1/2$. The fundamental alcove sequences under consideration are then

$$\alpha_* = (-t, 0, 0, t), \qquad \beta_* = (-t, 0, 0, t),$$

$$\gamma_* = (\gamma_1 \le \gamma_2 \le \gamma_3 \le \gamma_4),$$

and the inequalities given by combining Theorem 16 with Figure 10 and the above alcove sequences are

$$\begin{aligned} \gamma_1 + 2t &\ge 0, & \gamma_1 + \gamma_2 + 2t &\ge 0, & -\gamma_4 + 2t &\ge 0,\\ \gamma_2 + t &\ge 0, & \gamma_1 + \gamma_4 + t &\ge 0, & -\gamma_3 + t &\ge 0,\\ \gamma_3 &\ge 0, & \gamma_1 + \gamma_4 - 2t &\ge -1, & -\gamma_2 &\ge 0,\\ \gamma_1 - t &\ge -1, & \gamma_2 + \gamma_3 - 2t &\ge -1, & -\gamma_4 - t &\ge -1. \end{aligned}$$

From these inequalities, we may draw the following consequence:

[13] As an interesting aside, SWAP lies outside of this polytope.

[14] Of course, this is not automatically true: these subpolytopes could form something like a "foliation" of $\operatorname{LogSpec}\gamma(P^2_{\mathrm{XY}})$.

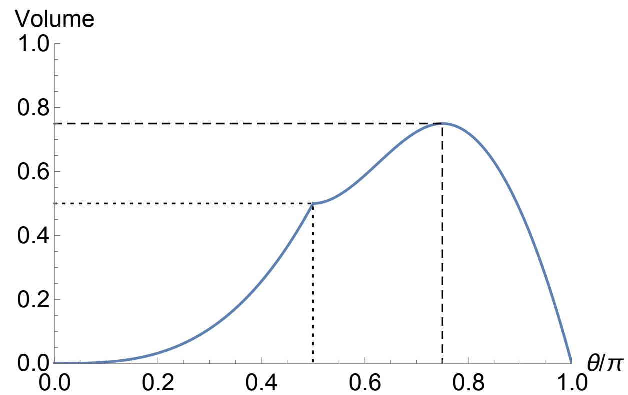

FIG. 4. Volume of $\operatorname{LogSpec}\gamma(P^2_{\mathrm{XY}_\theta})$, plotted as a fraction of the volume of $\mathfrak{A}_{C_2}$ against θ/π.

Theorem 32. *The volume of* $\operatorname{LogSpec}\gamma(P^2_{\mathrm{XY}_\theta})$ *is maximized at* $\theta = 3\pi/4$.

Proof. Because the finite family of inequalities determining $P(\theta) = \operatorname{LogSpec}\gamma(P^2_{\mathrm{XY}_\theta})$ are linearly dependent in θ, the curve $\operatorname{vol} P(\theta)$ is piecewise cubic in θ. Writing $t = \theta/\pi$, one can use this fact, together with sampling [13] and interpolation techniques, to determine a formula for $\operatorname{vol} P(t)$:

$$\operatorname{vol} P(t) = \begin{cases} 4t^3 & 0 \le t \le 1/2,\\ 15/2 - 36t + 60t^2 - 32t^3 & 1/2 \le t \le 3/4,\\ -6 + 18t - 12t^2 & 3/4 \le t \le 1, \end{cases}$$

as depicted in Figure 4. From this curve, we may directly determine its maximum value. □

Remark 33. In Figure 5, Figure 6, and Figure 7, we illustrate the solids $\operatorname{LogSpec}\gamma(P^2_{\mathrm{XY}_\theta})$ for varying values of θ, where we have projected onto the last three coordinates and shaded $\mathfrak{A}_{C_2}$ red. The solids themselves display some interesting behavior. First, for $0 \le \theta \le \theta' \le 3\pi/4$, there is an inclusion of solids $\gamma(P^2_{\mathrm{XY}_\theta}) \subseteq \gamma(P^2_{\mathrm{XY}_{\theta'}})$, from which it follows that $\operatorname{vol}\gamma(P^2_{\mathrm{DB}}) \ge \operatorname{vol}\gamma(P^2_{\mathrm{XY}_\theta})$ for any $0 \le \theta \le 3\pi/4$ as in the Theorem. However, for $3\pi/4 \le \theta < \theta' \le \pi$, neither of $\gamma(P^2_{\mathrm{XY}_\theta})$ and $\gamma(P^2_{\mathrm{XY}_{\theta'}})$ is contained in the other: although $\gamma(P^2_{\mathrm{XY}_\theta})$ continues to lose volume as θ approaches π from the left, the solid also continues to pick up "new" two-qubit programs as it shrinks.

Definition 34. Motivated by Theorem 32, we also refer to $\mathrm{XY}_{\frac{3\pi}{4}}$ by the briefer synonym DB [15].

It is then of further interest to give a precise description of the polytope $\operatorname{LogSpec}\gamma(P^2_{\mathrm{DB}})$.

[15] Dagwood Bumstead is a comic strip character famous for making really big sandwiches.

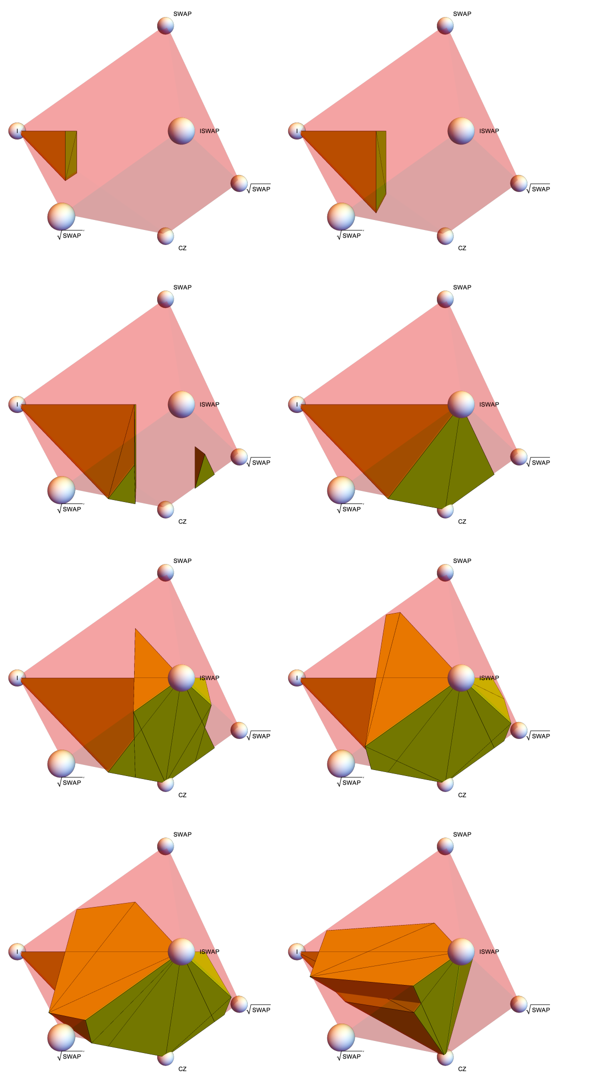

FIG. 5. The solids $\operatorname{LogSpec}\gamma(P^2_{\mathrm{XY}_{\pi t}})$ for differing values of t: 2/10, 3/10, ..., 9/10.

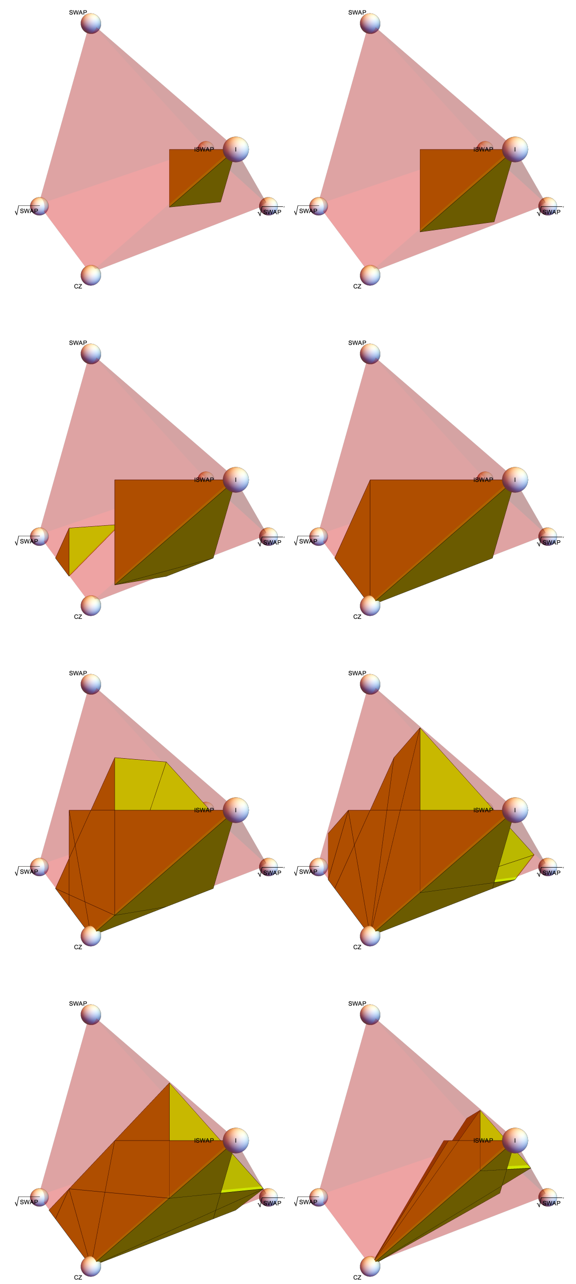

FIG. 6. The solids $\operatorname{LogSpec}\gamma(P^2_{\mathrm{XY}_{\pi t}})$, as shown from a second perspective, for differing values of t: 2/10, 3/10, ..., 9/10.

Lemma 35. $\operatorname{LogSpec}\gamma(P^2_{\mathrm{DB}})$ *is a union of two convex polytopes, respectively described the following two families of inequalities:*

$$\left\{\gamma_3 \geq 0,\ \frac{1}{4} \geq |\gamma_2 + \gamma_3|,\ 0 \geq \gamma_2\right\},$$

$$\left\{\frac{1}{2} \geq \gamma_2 + \gamma_3 + \gamma_4,\ -\frac{1}{4} + \gamma_3 + \gamma_4 \geq 0,\ \frac{1}{4} \geq |\gamma_2 + \gamma_3|\right\}$$

each together with the inequalities specifying the fundamental alcove. The extremal points of the first polytope are

$$\left(-\frac{1}{4}, -\frac{1}{4}, \frac{1}{4}, \frac{1}{4}\right), \quad \left(-\frac{1}{6}, -\frac{1}{6}, 0, \frac{1}{3}\right), \quad (0,0,0,0),$$
$$\left(-\frac{5}{8}, -\frac{1}{8}, \frac{3}{8}, \frac{3}{8}\right), \quad \left(-\frac{1}{2}, 0, \frac{1}{4}, \frac{1}{4}\right), \quad \left(-\frac{1}{2}, 0, 0, \frac{1}{2}\right),$$
$$\left(-\frac{5}{8}, 0, \frac{1}{4}, \frac{3}{8}\right),$$

and those of the second polytope are

$$\left(-\frac{1}{8}, -\frac{1}{8}, \frac{1}{8}, \frac{1}{8}\right), \quad \left(-\frac{3}{8}, \frac{1}{8}, \frac{1}{8}, \frac{1}{8}\right), \quad \left(-\frac{1}{2}, \frac{1}{8}, \frac{1}{8}, \frac{1}{4}\right),$$
$$\left(-\frac{1}{4}, -\frac{1}{4}, \frac{1}{4}, \frac{1}{4}\right), \quad \left(-\frac{1}{2}, 0, \frac{1}{4}, \frac{1}{4}\right), \quad \left(-\frac{1}{2}, -\frac{1}{6}, \frac{1}{3}, \frac{1}{3}\right),$$

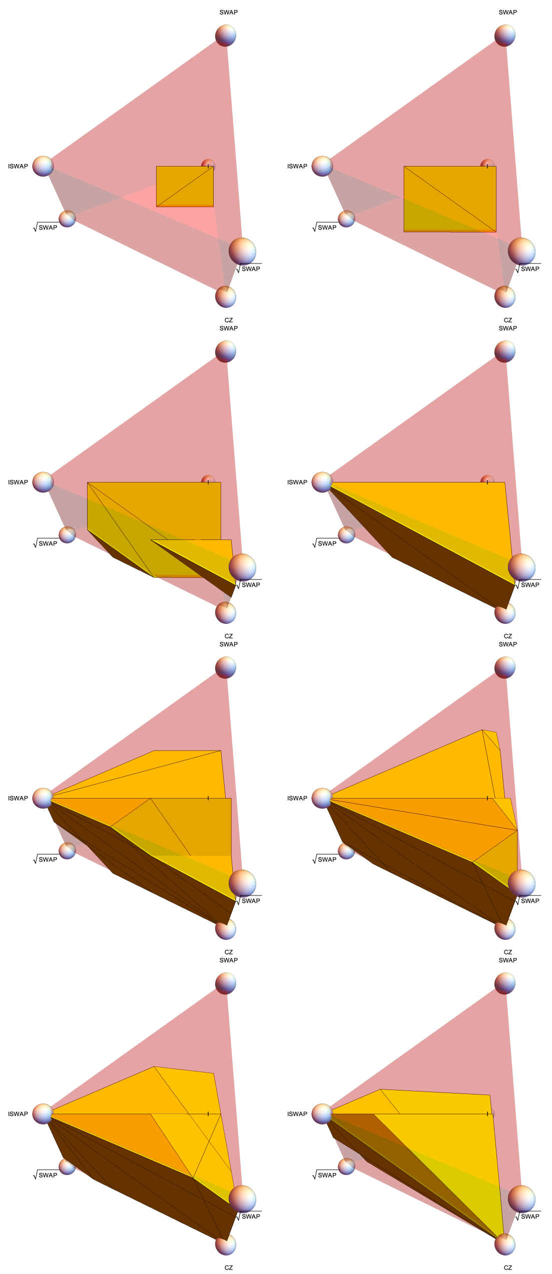

FIG. 7. The solids $\operatorname{LogSpec}\gamma(P^2_{\mathrm{XY}_{\pi t}})$, as shown from a third perspective, for differing values of t: 2/10, 3/10, . . . , 9/10.

$$\left(-\frac{1}{8}, -\frac{1}{8}, -\frac{1}{8}, \frac{3}{8}\right), \quad \left(-\frac{1}{2}, 0, 0, \frac{1}{2}\right).$$

Proof. The family of inequalities comes directly from reducing the family supplied by Appendix A. After calculating all of the points of intersection of the associated equalities and discarding those intersection points which do not satisfy all of the inequalities, the remainder is the set of extremal vertices, as listed above. □

Remark 36. The polytope $\operatorname{LogSpec}\gamma(P^2_{\mathrm{DB}})$ is pictured from three angles in Figure 8.

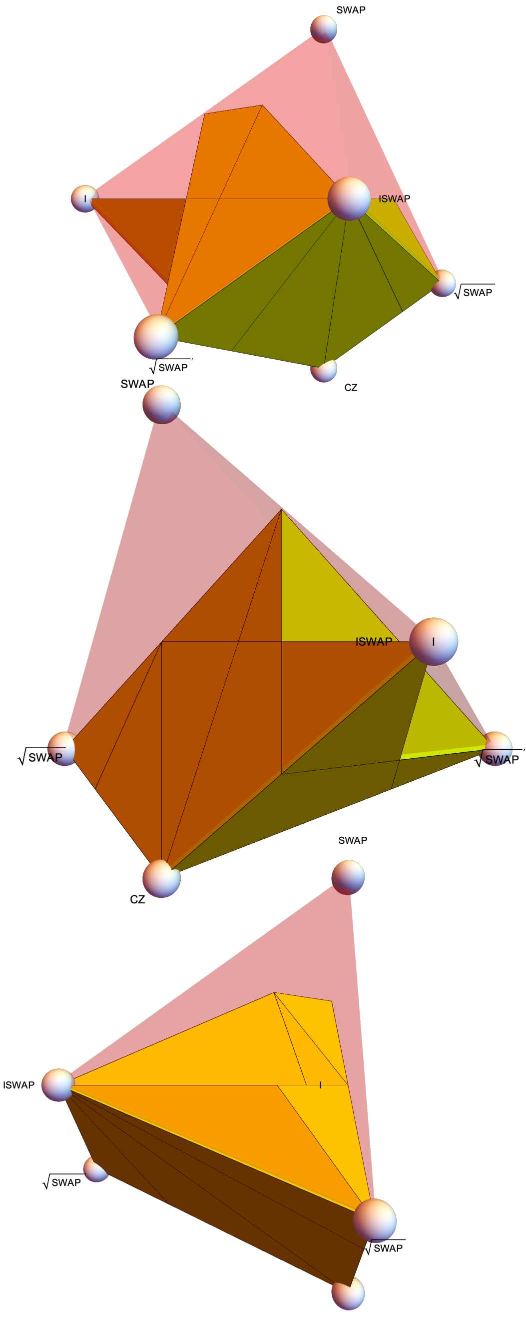

FIG. 8. Three views of $\operatorname{LogSpec}\gamma(P^2_{\mathrm{DB}})$

Remark 37. For the interested reader, we also include as Figure 9 a depiction a numerical sampling of $\operatorname{vol}\operatorname{LogSpec}\gamma(P^2_X)$ as X ranges over (the facets of) the entire monodromy polytope. Points shaded black correspond to those values of X for which $\operatorname{vol}\operatorname{LogSpec}\gamma(P^2_X)$ is at 0% of the total volume, and points shaded white correspond to 100% of the total volume. In the middle figure, the heat values along the line connecting the westernmost point, labeled I, to the center point, labeled iSWAP, correspond to the graph depicted in Figure 4.

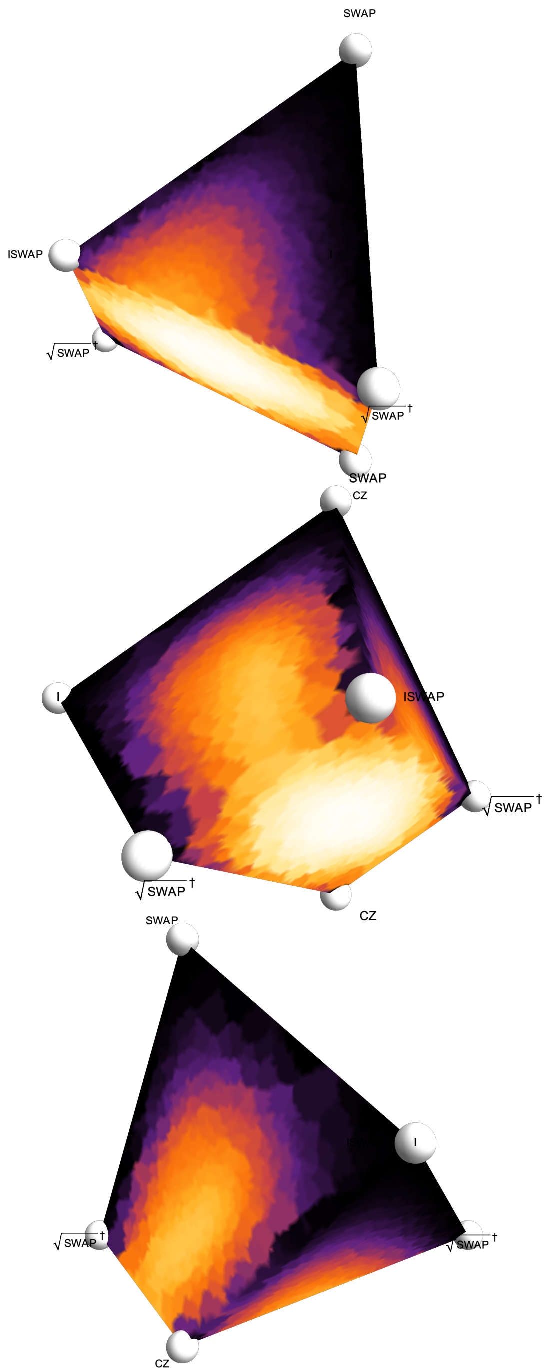

FIG. 9. An approximate heat map of volumes of symmetric monodromy polytope slices. The vertices of the figures are labeled I, CZ, iSWAP, SWAP, and $\sqrt{\text{SWAP}}$. A gate U is shaded according to the volume of $\operatorname{LogSpec}\gamma(P_U^2)$: black is 0% of the total volume of $\mathfrak{A}_{C_2}$, and white is 100%.

VI. APPROXIMATE COMPILATION

We now use the above descriptions of the polytopes P_S^n to address the problem of *approximate compilation*:

Problem 38. Given a two-qubit program U and a gate set S whose members $s \in S$ have associated fidelity estimates f_s, what circuit drawn from S gives the greatest fidelity approximation to U?

For instance, in this specific setting of $S = \{\text{CZ}\}$, Lemma 20 shows that every such U can be written as a circuit involving three applications of CZ, whereas Lemma 19 shows that almost no U can be decomposed exactly using just two applications of CZ. Nonetheless, if there is an associated cost to each application of CZ, it may be preferable to deliberately "miss" U (and thereby incur deliberate error) if it affords an opportunity to avoid applying CZ a third time (and thereby avoid indeliberate error). This idea of approximate compilation is not a new one [14, Appendix B], and we begin by recalling some useful results.

Definition 39 ([15], see also [16])**.** Given a pair of two-qubit programs G and G', we define their *average gate fidelity* to be

$$F_{\text{avg}}(G, G') = \int_{\chi \in \mathbb{P}(V)} |\langle \chi | G^\dagger G' | \chi \rangle|^2$$
$$= \frac{4 + |\operatorname{tr}(G^\dagger G')|^2}{4 \cdot 5} \in [1/5, 1].$$

Because this comes down to a trace calculation, this value is especially easy to calculate for simultaneously diagonalizable gates, which includes pairs of canonical gates after conjugation by Q:

Lemma 40 ([14, Equation B.8d])**.** *Let* $G = \text{CAN}(\alpha, \beta, \gamma)$ *and* $G' = \text{CAN}(\alpha', \beta', \gamma')$ *be two canonical gates with parameter differences*

$$\Delta_\alpha = \frac{\alpha' - \alpha}{2}, \qquad \Delta_\beta = \frac{\beta' - \beta}{2}, \qquad \Delta_\gamma = \frac{\gamma' - \gamma}{2}.$$

Their average gate fidelity is given by

$$20 F_{\text{avg}}(G, G') = 4 + 16 \left| \begin{matrix} \cos\Delta_\alpha \cos\Delta_\beta \cos\Delta_\gamma \\ + \\ i \sin\Delta_\alpha \sin\Delta_\beta \sin\Delta_\gamma \end{matrix} \right|. \square$$

In pursuit of Problem 38, we are also interested in the effect of local gates on Lemma 40. Rewriting the trace in terms of Q–conjugates, we have

$$|\operatorname{tr} GG'|^2 = |\operatorname{tr} L_2^\dagger C^\dagger L_1^\dagger \cdot L_1' C' L_2'|^2 = |\operatorname{tr} D_1 O_1 D_2 O_2|^2,$$

where $D_1 = (C^\dagger)^Q$ and $D_2 = (C')^Q$ are diagonal gates and $O_1 = (L_1^\dagger L_1')^Q$ and $O_2 = (L_2' L_2^\dagger)^Q$ are orthogonal gates. Letting L_2 and L_2' range, we see from Corollary 11 that we are maximizing a quadratic functional over the monodromy polytope slice associated to D_1 and D_2. Mercifully, one need not employ this heavy machinery to solve this optimization problem:

Lemma 41 ([17, Section III.A])**.** *Suppose that* C_1, C_2 *are fixed canonical gates and that* L_1, L_1' *are fixed local gates. Letting* L_2 *and* L_2' *scan over all local gates, the value* $F_{\text{avg}}(L_1 C_1 L_1', L_2 C_2 L_2')$ *is maximized when taking* $L_2 = L_1$ *and* $L_2' = L_1'$. $\square$

Corollary 42. *The spectrum of the gate which gives the best approximation to a two-qubit unitary U depends only on* $\mathrm{LogSpec}\,\gamma(U)$. □

By combining these results to our descriptions of P_S^n for our preferred gate sets S, we produce the following protocol for approximate compilation. In the following, we take S to be a gate-set with the nesting property of Corollary 17 and U to be a two-qubit program to be compiled.

1. Calculate the canonical decomposition associated to U: $U = LCL'$.
2. Let $n = 1$.
3. Use $\mathrm{LogSpec}\,\gamma(U)$ to calculate the point $\gamma_*^n \in \mathrm{LogSpec}\,\gamma(P_S^n)$ which maximizes $F_{\mathrm{avg}}(U, -)$. Multiply this value by f_S^n [16].
4. Is this fidelity value smaller than the previous fidelity value? If not, increment n and try Step 3 again. Otherwise, proceed to Step 5.
5. Find a realization R of γ_*^{n-1} with canonical decomposition
$$R = L_{\mathrm{approx}} \cdot C_{\mathrm{approx}} \cdot L'_{\mathrm{approx}}.$$
6. Return
$$LL_{\mathrm{approx}}^\dagger \cdot R \cdot (L'_{\mathrm{approx}})^\dagger L'.$$

The first half of the protocol depends only on the structure of the polytopes P_S^n, from which we may conclude the following result:

Corollary 43. *The two-qubit gate sets* {CZ}, {*i*SWAP}, {CPHASE}, *and* {PSWAP} *all do an equally effective job of approximating an arbitrary two-qubit program by a circuit of multiqubit depth* 2.

Proof. This is a direct consequence of coupling the above ideas to Lemma 19, Lemma 23, Lemma 30, and Lemma 31. □

Remark 44 ([14, Appendix B]). Finding the nearest point in P_S^n to an arbitrary outside point is numerically accessible, but it does not usually admit a closed-form solution. An exception is the case of P_{CZ}^2, where the nearest canonical gate to $\mathrm{CAN}(\alpha, \beta, \gamma)$ is $\mathrm{CAN}(\alpha, \beta, 0)$.

[16] We are using f_S^n as an *approximation* for the fidelity of the depth n circuit. However, as no form of fidelity is multiplicative, there is considerable room for the implementer to express her own preference here.

Example 45. The SWAP gate is of particular interest, and so we provide an analysis of its approximants as an example of these methods. The nearest point to SWAP within $\mathrm{LogSpec}\,\gamma(P_{\mathrm{DB}}^2)$ is $(-1/3, 0, 1/6, 1/6)$, with an average gate infidelity of 3/20. Remarkably, this is also nearest point within $\bigcup_\theta \mathrm{LogSpec}\,\gamma(P_{\mathrm{XY}_\theta}^2)$ (i.e., over all possible choices of fixed values of θ), and in fact this point belongs to the polytopes associated to the fixed values of $t = \theta/2\pi$ in the range $[1/3, 5/6]$. For contrast, the nearest point to $\mathrm{SWAP} \equiv \mathrm{CAN}(\pi/2, \pi/2, \pi/2)$ within $\mathrm{LogSpec}\,\gamma(P_{\mathrm{CZ}}^2)$ is given by $\mathrm{CAN}(\pi/2, \pi/2, 0)$, with an average gate infidelity of 8/20.

VII. OPEN QUESTIONS

In closing the main thread of the paper, we list some follow-on projects to this paper where we expect to find interesting results.

A. Algorithmic effectiveness and circuit realization

The single most important avenue left open by this work is the actual manufacture of a circuit in P_X^2 from a point in $\mathrm{LogSpec}\,\gamma(P_X^2)$, which we refer to as the *realization problem.*

- Edelman et al. have presented a specialization of Newton's method on a curved Riemannian manifold to the orthogonal group with its natural metric [18]. If one were able to provide approximate solutions to the realization problem, such an algorithm could be used to rapidly increase the accuracy of such a solution—but without approximate solutions, such methods have no guarantee of convergence [17]. Additionally, this method would require foreknowledge of the gates D_E and D_F in Problem 8, limiting its applicability in parametric settings such as P_{XY}^2.
- From the perspective of Appendix A, a solution to the monodromy problem corresponds to a flat connection on the trivial $PU(4)$–bundle over a punctured Riemann sphere with prescribed monodromy values. The data of an *arbitrary* connection is easier to describe: it assigns to each path an element of $PU(4)$ via parallel transport, perhaps with some further smoothness conditions. The Rade's thesis [19] analyzes the Yang–Mills flow from an arbitrary such connection (with boundary conditions) to a flat representative, and for generic connections

[17] In the particular case of P_{XY}^2, M. Scheer has pointed out to us the commutation relation $[\mathrm{XX}+\mathrm{YY}, \mathrm{ZI}+\mathrm{IZ}] = 0$, from which it follows that the group of interest can be reduced from $PO(4)$ to a particular four-dimensional subset.

its convergence is rapid. One might therefore try to discretize the punctured Riemann sphere and apply a numerical variant of Rade's method. It is not immediately clear, however, how one would introduce the orthogonality constraints present in Problem 8.

- Cole Franks et al. [20, 21] have described effective numerical methods for solving the *additive* analogue of the eigenvalue problem. One might explore multiplicative variations on their methods (especially those with the orthogonality constraint kept in mind) which would then adapt to solve the problem posed here.

B. Alternative interpretations of "maximum"

The particular metric by which we measured the particular utility of DB over other instances of XY_θ was the volume of the polytope $\mathrm{LogSpec}\,\gamma(P^2_{\mathrm{DB}})$. It is not clear that this is the best such metric (nor that there is a best). Some alternative metrics that seem worth exploring include:

- Is there a value of θ for which the average (or worst) value of average gate infidelity is minimized? Against this metric, an "elliptical" polytope may be more valuable than a "spherical" one. This analysis may also change when considering other approximation metrics than average gate infidelity, e.g., a diamond distance.
- The Haar volume (or, indeed, most any other natural volume) of a subset of $PU(4)$ is not perfectly related to the volume of its image as a subset of $\mathfrak{A}_{C_2}$. For any such volume vol' on $PU(4)$, it would also be of interest to maximize the analogous function $\mathrm{vol}'\, P^2_{\mathrm{XY}_t}$ over t. (For the Haar volume, it appears that the maximum remains at $\theta = 3\pi/4$, but we do not have a proof that this is so.)

It would also be of interest to understand the local behavior of any of these metrics with respect to small distances in $PU(4)$. This is the domain of *coherent unitary error*, and one might hope to leverage some of the results of this paper to tailor a compilation method for an error-prone device. Preliminary inspection of this for P^2_{CZ} indicates that derivatives conspire so that only large coherent unitary error gives rise to significant gain in volume.

C. Unexplored polytopes

The material presented here amounts to a toolkit for analyzing the space of programs available to a given native gate set. We have used this as incentive to investigate a particular native gate set because of its depth-two behavior and its relevance to a particular sort of hardware, but this is hardly the only option.

- Produce concise descriptions of some of the standard polytopes not fully exposed in this paper (e.g., P^2_{XY}, $P^2_{\{\mathrm{CPHASE}, i\mathrm{SWAP}\}}$, $\ldots$).
- Describe those native gate sets S which enjoy $P^2_S = \mathfrak{A}_{C_2}$. This set is nonempty, as the B–gate has this property. Are there other singletons? Other finite sets?
- We have avoided checking whether $P^3_{\mathrm{DB}} = \mathfrak{A}_{C_2}$. We certainly expect this to be so, but the associated system of inequalities exhausts both us and our computer algebra systems.

D. Leakiness

The analysis of "leaky gates" in Appendix B is not as thorough as it might be. Here are some open questions concerning that property:

- In Remark 64, we argue that within the local equivalence class of a leaky entangler, there is one where the single-qubit gates involved in the leakiness relation are all Z–gates. However, their parameters may depend on each other in a nontrivial way. Give a description of the possible ways this can happen. The exponential family SWAP_θ (i.e., the θ^{th} root of SWAP) is probably of interest here.
- Every given example of a leaky gate is leaky on both coordinates. Is this always the case?
- Every given example of a leaky gate is transpose-symmetric. Is this always the case?
- Prove the subspace of leaky entanglers coincides exactly with the edges of $\mathfrak{A}_{C_2}$.

ACKNOWLEDGEMENTS

We would like to thank Rigetti Computing for providing such a stimulating workplace, with difficult problems to solve and wonderful peers to work alongside. In particular, J. Combes, E. Davis, C. Hadfield, P. Karalekas, A. Papageorge, N. Rubin, C. Ryan, M. Scheer, M. P. da Silva, M. Skilbeck, and N. Tezak contributed a lot to our momentum, whether through pointers, proofreading, or generalized enthusiasm. E. Davis deserves special credit, as he finally put us on the right path to move from numerical experiment to mathematical proof, and this project might not have come together if not for his crucial advice. Although W. Zeng had been suggesting that we think about approximate compilation for some time, Section VI is a direct result of A. Javadi-Abhari's very pleasant talk at IWQC 2018. We additionally had the pleasure of speaking with the mathematicians W. C. Franks, B. Gammage, S. Kumar, E. Lerman, P. Solis, R. Wentworth, and C. Woodward, who freely offered their consultation and expertise on matters related to the monodromy polytope. The first author would like to note further the indirect but invaluable role that his PhD adviser, C. Teleman, played in this project: the material presented here is *much* closer to Teleman's domain than the first author's thesis ever was, and acquiring the working knowledge to complete this project would have been much harder without a steady exposure to these ideas over the years. Finally, an additional hearty thank you to R. Bryant for teaching the first author most of what he knows about Lie theory (and from the second author to the first for the same reason).

Appendix A: The mathematics of the monodromy polytope

In this appendix, we produce some of the details (or, failing that, some soothing exposition) of the mathematics underlying our results in the main text. This effort cleaves into two parts: some generic convexity results in symplectic geometry that give the qualitative solution to the multiplicative eigenvalue problem (and which merit the name "monodromy polytope"), followed by some results around quantum cohomology that give the quanitative solution.

1. Qualitative results

Before getting involved with the multiplicative eigenvalue problem directly, we first give a slightly ahistorical account [18] of a generic qualitative result found in symplectic geometry.

Definition 46. A *symplectic manifold* M is an oriented $2n$–manifold equipped with a choice of *symplectic form* ω, which is an n^{th} root of the volume form (or, equivalently, an everywhere nondegenerate 2–form).

Example 47. Examples of such objects are rife in physics: all phase spaces are instances of symplectic manifolds. For an ultra-simple but ultra-concrete example, we might take $M = \mathbb{R}^2$ with the symplectic form $\omega = dp \wedge dq$, or more generally $M = \mathbb{R}^{2d}$ with $\omega = \sum_j dp_j \wedge dq_j$. These arise as the phase spaces associated to d many noninteracting particles on a line. In general, a symplectic manifold has this as its local form.

Definition 48. Given an action on a symplectic manifold M by a Lie group G, a *moment map* is a G–equivariant function $\Phi\colon M \to \mathfrak{g}^*$, where the target is imbued with the coadjoint action.

Example 49. Again, examples of such objects are rife in physics: a nontrivial gauge group gives rise to a G–action on a manifold, and a moment map can be used to describe a G–invariant physical quantity, such as the total energy of a system. In the above example, $G = S^1$ acts on $\mathbb{R}^2$ by rotation, and the associated Lie algebra $\mathfrak{g}^*$ can be identified with $\mathbb{R}$ in such a way that a moment map is given by $\Phi(v) = \frac{1}{2}|v|^2$. Similarly, the d–torus $G = (S^1)^{\times d}$ acts on $\mathbb{R}^{2d}$ by rotations of the component planes, and there is an associated moment map $\mathbb{R}^{2d} \to \mathfrak{g}^* \cong \mathbb{R}^d$ which sends each particle to its kinetic energy.

A useful tool for manufacturing these objects comes in the form of the following theorem:

Theorem 50 (Symplectic reduction)**.** *Let M be a symplectic G–manifold with associated proper moment map Φ_G, and let $H \leq G$ be a normal subgroup. When $M/\!\!/G := \Phi_G^{-1}(0)/H$ is a manifold, it inherits both a symplectic form (which pulls back to $\Phi_G^{-1}(0)$ to agree with the restriction of ω_M) and a compatible action by G/H and moment map $\Phi_{G/H}$.* □

Our interest in these objects stems from the following family of convexity results:

Theorem 51. *Let G be a Lie group and let M be a connected Hamiltonian G–manifold with proper moment map $\Phi\colon M \to \mathfrak{g}^*$.*

- *(Atiyah [25], Guillemin–Sternberg [26, 27]:) Suppose that $G = T$ is a compact torus, and let A be a choice of fundamental alcove within T. The restriction of the image of Φ to A then forms a convex polytope.*
- *(Kirwan [28]:) Suppose that G is compact, let $T \leq G$ be a choice of maximal torus with corresponding dual Cartan subalgebra $\pi\colon \mathfrak{g}^* \to \mathfrak{t}^*$, and let A again be a fundamental alcove within $\mathfrak{t}^*$. The restricted set $A \cap \operatorname{im}(\pi \circ \Phi)$ is a convex polytope.*
- *(Meinrenken–Woodward [29, Theorem 3.13]:) Suppose that $G = LG'$ for G' a compact, connected, simply connected Lie group, let T' be a choice of maximal torus within G', and let A' be a choice of fundamental alcove within $(\mathfrak{t}')^*$. The intersection $\Phi(M) \cap A'$ is then a convex polytope [19].* □

[18] The solution to this problem is strongly coupled to the solution of the corresponding "linearized" problem: given Hermitian matrices H_1 and H_2, what spectra can possibly arise as the operator spectrum of $\mathrm{Ad}_{U_1} H_1 + \mathrm{Ad}_{U_2} H_2$ for unitary operators U_1 and U_2? A conjectural solution to this problem was set out by Horn [22], which spurred the development of a great many results in symplectic geometry and representation theory in an effort to explain his findings, and these tools were ultimately used by Klyachko [23] to settle the matter. Knutson [24] gives a very pleasant overview of this body of work and its surroundings, and although he does not address the multiplicative problem, (generalizations of) these same tools reappear in this context. We intend the word "ahistorical" only in the sense that the tools were developed *in response to* the visible behavior of the (additive) eigenvalue problem, whereas our exposition presents the tools as generic ideas which we then apply *post facto* to the eigenvalue problem—a significant misrepresentation of history.

[19] Additionally: for any face σ of A' such that $\Phi(M) \cap \sigma \neq \emptyset$, the

Remark 52. The most basic of this chain of results is somewhat believable: in Example 49, the image of the moment map is the positive orthant in $\mathfrak{t}^*$. Since a general symplectic manifold is constructed locally from that example, the image of a general moment map is constructed locally out of such "corners"—though amplifying this to an equivariant statement (and then to the nonabelian setting) is no trivial feat. The final form of the theorem is *considerably* harder to visualize, but it is the version that will concern us chiefly.

Example 53 ([30, p. 587], [31]). We focus our attention on an example that physicists will recognize as an instance of Yang–Mills theory. Let G be a compact connected Lie group (e.g., $SU(4)/C_2$) with compact simply-connected cover (e.g., $SU(4)$), let Σ be Riemann sphere with b disks excised, and let P be the trivial principal G–bundle over Σ. The space $\mathcal{A}(\Sigma)$ of $\mathfrak{g}$–valued connections on P may be identified with $\Omega^1(\Sigma; \mathfrak{g})$, and it can be shown to carry the structure of a symplectic manifold using the Atiyah–Bott symplectic form

$$\omega_{AB}(A_1, A_2) = \int_\Sigma a_1 \wedge a_2.$$

This carries a compatible action by the gauge group $\mathcal{G}(\Sigma)$ of sections of P (i.e., G–valued continuous functions on Σ), which has Lie algebra $\Omega^0(\Sigma, \mathfrak{g})$, and this action moreover admits a moment map Φ_{AB} determined by

$$\langle \Phi_{AB}(A), \xi \rangle = \int_\Sigma F_A \cdot \xi + \int_{\partial\Sigma} \iota^*(A \cdot \xi),$$

where F_A is the curvature form associated to A and $\iota\colon \partial\Sigma \to \Sigma$ is the inclusion of the boundary components. Writing $\mathcal{G}_\partial(\Sigma)$ for the term in the kernel sequence

$$1 \to \mathcal{G}_\partial(\Sigma) \to \mathcal{G}(\Sigma) \xrightarrow{\iota^*} \mathcal{G}(\partial\Sigma) \to 1,$$

the restricted action on $\mathcal{A}(\Sigma)$ inherits the moment map $\Phi_\partial(A) = F_A$, and so the symplectic reduction

$$\mathcal{M}^\flat(\Sigma) = \mathcal{A}(\Sigma) /\!\!/ \mathcal{G}_\partial(\Sigma) = \mathcal{A}^\flat(\Sigma)/\mathcal{G}_\partial(\Sigma),$$

called the *moduli of flat connections*, inherits an action by $\mathcal{G}(\partial\Sigma) \cong LG^b$ and a moment map $\Phi^\flat(A) = \iota^* A$.

Corollary 54 ([32, Theorem 3.2], [29, Theorem 3.16])**.** *The set*

$$\operatorname{LogSpec}\{U_1, U_2, U_3 \in SU(4) \mid U_1 U_2 = U_3\} \subset \mathfrak{A}^{\times 3}$$

is a convex polytope.

Construction. We set $\Sigma = \mathcal{P}^1 \setminus \{1, 2, 3\}$ and $G = SU(4)/C_2$, then apply Example 53 to conclude that $\mathcal{M}^\flat(\Sigma)$ is a symplectic manifold with associated moment map $A \mapsto \iota^* A$. Fix the following auxiliary data:

- Parametrizations $B_j\colon S^1 \to \Sigma$ of the j^{th} boundary component.
- Paths $\gamma_j\colon B_1(0) \to B_j(0)$ such that $\pi_1\Sigma$ is generated by $\gamma_j^{-1} B_j \gamma_j$, subject to the relation

$$\prod_{j=1}^3 \gamma_j^{-1} B_j \gamma_j = 1.$$

A connection A associates to these data elements $\operatorname{Mon}(B_j) = B_j^* A \in L\mathfrak{g}^*$, the monodromy of A about B_j, and $\Gamma(\gamma_j)_0^1$, the action of parallel transport along γ_j from the fiber over $\gamma_j(0)$ to the fiber over $\gamma_j(1)$.

It is well-known that the space of flat connections on a trivial G–bundle is equivalent to the space of G–representations of the fundamental group of the base, which in the case of Σ is

$$\pi_1\Sigma = \left\langle \begin{array}{c} b_1 = B_1, b_2 = \gamma_2^{-1} B_2 \gamma_2, \\ b_3 = \gamma_3^{-2} B_3 \gamma_3 \end{array} \middle| 1 = b_1 b_2 b_3 \right\rangle.$$

The procedure for extracting such a representation is by sending a loop in the base to the monodromy of the connection around the loop. One may augment this idea into a commuting square of identifications

$$\begin{array}{ccc} \mathcal{M}^\flat(\Sigma) & \to & \left\{ \begin{array}{c} c_* \in \{1\} \times G^2 \\ \xi_* \in (L\mathfrak{g}^*)^{\times 3} \end{array} \middle| 1 = \prod_{j=1}^3 \operatorname{Ad}_{c_j} \operatorname{Mon}(\xi_j) \right\} \\ \downarrow \Phi & & \downarrow \Phi \\ \operatorname{Lie} \mathcal{G}(\partial\Sigma) & \longrightarrow & \left\{ (\xi_*) \in (L\mathfrak{g}^*)^{\times 3} \right\}, \end{array}$$

where the first horizontal arrow is defined by

$$c_j(A) = \Gamma(\gamma_j)_0^1, \qquad \xi_j(A) = B_j^*(A),$$

the monodromy operator is defined by

$$\operatorname{Mon}(\xi_j) = \int_{B_j} B_j^*(A) \in G,$$

the second horizontal arrow is given by B_j^*, and the action of $\mathcal{G}(\partial\Sigma) \cong LG^3$ on the top-right corner is given by

$$g \cdot c_j = g_j(0)^{-1} c_j g_1(0), \quad g \cdot \xi_j = \operatorname{Ad}_{g_j} \xi_j - g_j^{-1} d g_j.$$

The meat of this proof then argues that this particular form of the equivalence is, in fact, an equivariant symplectomorphism.

Granting this, we find ourselves at the doorstep of the multiplicative eigenvalue problem. Note first that the operator Mon enjoys two pleasant properties:

1. After using the Killing form to identify $\mathfrak{g}^*$ with the subspace $\mathfrak{g} \subseteq L\mathfrak{g}$ of constant loops, for $h \in \mathfrak{g}$ we have $\operatorname{Mon}(h) = \exp(h)$, the usual Lie exponential.
2. The G–action on ξ_j is then arranged so that the following formula holds:

$$\operatorname{Mon}(g \cdot \xi_j) = \operatorname{Ad}_{g_j(0)} \operatorname{Mon}(\xi_j).$$

---

corresponding symplectic cross-section Y_σ is finite dimensional and connected, and the fibers of Φ are connected.

These properties combine to give the required link. We apply Theorem 51: take $A \subset \mathfrak{t}^*$ to be diagonal matrices whose entries obey the criteria set out by Definition 12. The image of the moment map then becomes those logarithmic spectral triples (ξ_1, ξ_2, ξ_3) for which there exist unitary operators c_2, c_3 satisfying

$$e^{-2\pi i \xi_1} = c_2^{-1} e^{2\pi i \xi_2} c_2 \cdot c_3^{-1} e^{2\pi i \xi_3} c_3. \qquad \square$$

Remark 55. Throughout the main body of the paper, there are two Lie groups of interest: $PU(4) = U(4)/\mathbb{C}^\times$, which participates in a nontrivial central extension

$$1 \to C_4 \to SU(4) \to PU(4) \to 1,$$

and the double cover $SU(4)/C_2$ of $PU(4)$, which also participates in a nontrivial central extension

$$1 \to C_2 \to SU(4) \to SU(4)/C_2 \to 1.$$

In general, we may consider compact connected Lie groups G whose universal cover $\widetilde{G}$ participates in a finite central extension

$$1 \to F \to \widetilde{G} \xrightarrow{\pi} G \to 1.$$

The Lie algebras of $\widetilde{G}$ and G may be identified by π, and the image of the moment map Φ_G considered in Corollary 54 is then given by the union over $f \in F$ of the images of the moment maps $\Phi_{\widetilde{G},f}$, constructed analogously so as to detect products of the form $U_1 U_2 = f U_3$ with $U_1, U_2, U_3 \in \widetilde{G}$.

2. Quantitative results

We now turn to quantitative results: given that the solution set to the multiplicative eigenvalue problem forms a convex polytope, what polytope is it? As in the additive case, this problem passes through representation theory, and in the exposition about the qualitative problem we have already begun to make this contact: a flat connection on a trivial vector bundle is equivalent data to a representation of the fundamental group of the base, and flat connections modulo gauge equivalence correspond to representations up to choice of basis. A theorem of Narasimhan and Seshadri showed that unitary representations of the fundamental group of a compact Riemann surface correspond to "stable" holomorphic vector bundles over the surface [33]. A vector bundle V is said to be stable when its slope, $\mu(V) = \deg(V)/\operatorname{rank}(V)$, decreases when passing to any subbundle [20], and such bundles can be shown to admit a unique flat unitary connection [34], giving one direction of the correspondence.

[20] Informally, a stable bundle is "more ample" than any of its subbundles.

However, our surface of interest, $\Sigma = \mathbb{CP}^1 \setminus \{1,2,3\}$, is a *noncompact* Riemann surface [21]. Work of Mehta and Seshadri extends the above correspondence to the noncompact case: a *parabolic bundle* (on $\mathbb{CP}^1$) is a holomorphic vector bundle E, a choice of finite set $S \subset \mathbb{CP}^1$, a choice of flag $\{E_{s,i}\}$ for each $s \in S$, and a list of weights $\lambda_{s,j}$ satisfying the strings of inequalities

$$\lambda_{s,1} \geq \cdots \geq \lambda_{s,n} > \lambda_{s,1} - 1$$

and $\deg E + \lambda_{+,+} = 0$. A parabolic bundle is additionally said to be *semistable* when its *parabolic slope*, a modification of the slope of a holomorphic vector bundle that is offset by the choice of weights, decreases when passing to any subbundle (and appropriately restricting the parabolic structure). They then showed the following result:

Theorem 56 ([35])**.** *Fix a set S and a list of parabolic weights satisfying $\lambda_{s,i} \in [0,1) \cap \mathbb{Q}$. The moduli space of semistable parabolic bundles on $\mathbb{CP}^1$ with these weights is a normal, projective variety, homeomorphic to the moduli space of flat unitary connections over $\mathbb{CP}^1 \setminus S$ such that the monodromy operator U_s at s has* $\operatorname{LogSpec} U_s = (\lambda_{s,i})_i$. $\square$

Agnihotri and Woodward note that if the moduli of parabolic vector bundles is nonempty, then it contains the trivial bundle with flags chosen in general position, eliminating one source of complexity. However, what this theorem conspicuously does not assert is when the moduli of semistable parabolic bundles is *nonempty*. Their next move is to use a complicated form of intersection theory known as *quantum cohomology* both to check nonemptiness and to produce the bounding hyperplanes. The ultimate theorem statement is as follows:

Definition 57. For $r, k > 0$ be positive integers with $r + k = n$, we define $\mathcal{P}_{r,k}$ to be the set of partitions

$$\mathcal{P}_{r,k} = \{(I_1, \ldots, I_r) \in \mathbb{Z}^r \mid 0 \leq I_1 \leq \cdots \leq I_r \leq k\}.$$

Let $\operatorname{Gr}(r,k)$ be the Grassmannian of k–planes in $\mathbb{C}^n$. Fix any complete flag in $\mathbb{C}^n$:

$$\mathbb{C}^n = F_n \supset F_{n-1} \supset \cdots \supset F_0 = \{0\};$$

then for any partition $I \in \mathcal{P}_{r,k}$, we then define the corresponding *Schubert variety* to be

$$\sigma_I = \left\{ W \in \operatorname{Gr}(r,k) \mid \dim(W \cap F_{I_j}) \geq j \right\}.$$

The *Schubert cell* $C_I \subset \sigma_I$ is the complement of all lower-dimensional Schubert varieties contained in σ_I:

$$C_I = \bigcap_{\sigma_J \subset \sigma_I} \sigma_I \setminus \sigma_J.$$

[21] In fact, the fundamental groups of compact Riemann surfaces are all known: the surface Σ_g of genus has fundamental group the free group on letters $a_1, b_1, \ldots, a_g, b_g$ subject to the relation $1 = [a_1, b_1] \cdots [a_g, b_g]$. There is no g for which this looks like our desired free group on generators a, b, c subject to $abc = 1$.

From these, we define Schubert cycles $[\sigma_I]$ and $[C_I]$, as well as cohomology classes T_I Poincaré dual to $[\sigma_I]$.

Theorem 58 ([36, Theorem 5.3, Lemma 5.5])**.** *The moduli of semistable parabolic bundles with prescribed weights $\lambda_{s,i}$ is non-empty if and only if*

$$\sum_{s\in S}\sum_{i\in I_s}\lambda_{s,i}\le d$$

for all subsets I_s and integers d such that there exists a degree d map sending $s\in S$ to a general translate of the Schubert cell C_{I_s}.

Moreover, let d be the lowest degree of any map

$$\mu\colon \mathbb{CP}^1\to \mathrm{Gr}(r,k)$$

sending $s\in S$ to a general translate of σ_{I_s}. Then q^d is the maximal power of q dividing $\prod_{s\in S}T_{I_s}$ in the small quantum cohomology ring of $\mathrm{Gr}(r,k)$. □

It remains to give a description of quantum cohomology and to compute the (small) quantum cohomology ring of a Grassmannian. We follow a set of summary lectures by Fulton and Pandharipande [37]. Beginning with a sufficiently nice space X and for a choice of class $\beta\in H_2(X)$, one may construct a *moduli space of nodal curves* $\mathcal{M}_{g,S}(X,\beta)$ populated by triples (C,S,μ) consisting of a projective connective nodal curve C of genus g, a subset $S\subset C$ in the nonsingular locus, and a map $\mu\colon C\to X$ such that $\mu_*[C]=\beta$ and such that μ admits finitely many automorphisms. This space has a compactification $\overline{\mathcal{M}_{g,S}}(X)$, and hence its rational cohomology acquires Poincaré duality and a theory of intersection [38]. Using this, we define an invariant I_β associated to strings of S–labeled cohomology classes $\prod_{s\in S}\gamma_s\in H^{2*}(X)$:

$$I_\beta\left(\prod_{s\in S}\gamma_s\right):=\int_{\overline{\mathcal{M}_{0,S}(X,\beta)}}\prod_{s\in S}\rho_s^*(\gamma_s),$$

where ρ_s is the evaluation map

$$\begin{aligned}\rho_s\colon \overline{\mathcal{M}_{0,S}(X,\beta)}&\to X,\\ \mu&\mapsto \mu(s).\end{aligned}$$

This definition contains the following special case: using the classes T_I as a basis for $H^{2*}(X)$ and writing g^{ef} for the (operator) inverse of $g_{ef}=\int_X T_e\smile T_f$, we have

$$T_i\smile T_j=\sum_{e,f}I_0(T_iT_jT_e)g^{ef}T_f.$$

Motivated by this observation, we use nontrivial classes β to define the following "deformed product":

Definition 59. The product on $H^*\mathrm{Gr}(r,k)$ extends to a commutative $\mathrm{Z}[\![q]\!]$–bilinear product on $\mathrm{Z}[\![q]\!]\otimes H^*\mathrm{Gr}(r,k)$ by the formula

$$\begin{aligned}T_i*T_j&=\left(\sum_{\substack{\beta\in H^2(\mathrm{Gr}(r,k))\\ \beta\text{ “effective”}}}I_\beta(T_iT_jT_e)q^{\int_\beta T_1}\right)g^{ef}T_f\\ &=\left(\int_{\mathrm{Gr}(r,k)}T_iT_jT_e+I_{\sigma_1}(T_iT_jT_e)q\right)g^{ef}T_f\\ &=:\sum_{d,f}N_{ij}^{f,d}(r,k)\cdot q^dT_f,\end{aligned}$$

The structure coefficients $N_{ij}^{f,d}(r,k)$ are called *quantum Littlewood–Richardson coefficients* [22].

The quantum Littlewood–Richardson coefficients are connected to enumerative geometry, and one can use this to calculate them directly in small-index cases; they are connected to cohomology and so obey associativity-type relations; and it is possible to assemble both of these sources of information into an algorithm which recursively computes them [39, 40]. Since we are specifically interested in the case of $SU(4)$, we produce a table of the quantum Littlewood–Richardson coefficients appearing in the products on the small quantum cohomology rings for $\mathrm{Gr}(1,3)$, $\mathrm{Gr}(2,2)$, and $\mathrm{Gr}(3,1)$ in Figure 10.

Altogether, these results assemble into the following summary theorem, the form of which presented here is due to Belkale [23].

Theorem 60 ([36, Theorem 3.1], [41, Theorem 7])**.** *Let U_1, U_2, $U_3\in SU(n)$ satisfy $U_1U_2=U_3$, and let α_*, β_*, γ_* be the fundamental alcove sequence respectively associated to these unitaries through* LogSpec*. Select $r,k>0$ satisfying $r+k=n$, select $a,b,c\in\mathcal{P}_{r,k}$, and take $d\ge 0$; then if $N_{ab}^{c,d}(r,k)=1$, the following inequality must hold:*

$$d-\sum_{i=1}^r\alpha_{k+i-a_i}-\sum_{i=1}^r\beta_{k+i-b_i}+\sum_{i=1}^r\gamma_{k+i-c_i}\ge 0.\qquad (*)$$

Moreover, given alcove sequences α_*, β_*, γ_* for which $N_{ab}^{c,d}(r,k)=1$ implies Equation (*), then there exist U_1, U_2, U_3 with $U_1U_2=U_3$ and

$$\alpha_*=\mathrm{LogSpec}\,U_1,\quad \beta_*=\mathrm{LogSpec}\,U_2,\quad \gamma_*=\mathrm{LogSpec}\,U_3.$$

Remark 61 ([37, Proposition 12]). In the case of a Grassmannian, the small quantum cohomology ring can be fully calculated and presented in summary form:

$$qH^*\mathrm{Gr}(r,k)=\frac{\mathrm{Z}[\sigma_1,\dots,\sigma_k,q]}{\begin{pmatrix}S_{r+1}(\sigma),\dots,S_{n-1}(\sigma),\\ S_n(\sigma)+(-1)^kq\end{pmatrix}},$$

where $S_r(\sigma)=\det(\sigma_{1+j-i})_{i,j=1}^r$ is a certain determinantal class in the Chern classes $\sigma_i=c_i(\xi)$ of the tautological bundle ξ over $\mathrm{Gr}(r,k)$.

[22] For X with $\dim H^2(X)>1$, one must introduce more than one formal class q. After accounting for this, the definition presented here is robust for a fairly broad class of spaces X.

[23] The original Mehta–Seshadri theorem concerns unitary flat connections. Belkale also produced an alternative form of their theorem appropriate for flat connections which are special unitary [41, Appendix].

r	k	a	b	c	d	$N_{ab}^{c,d}(r,k)$
1	3	(0)	(0)	(0)	0	1
			(1)	(1)	0	1
			(2)	(2)	0	1
			(3)	(3)	0	1
		(1)	(1)	(2)	0	1
			(2)	(3)	0	1
			(3)	(0)	1	1
		(2)	(2)	(0)	1	1
			(3)	(1)	1	1
		(3)	(3)	(2)	1	1
2	2	(0, 0)	(0, 0)	(0, 0)	0	1
			(1, 0)	(1, 0)	0	1
			(1, 1)	(1, 1)	0	1
			(2, 0)	(2, 0)	0	1
			(2, 1)	(2, 1)	0	1
			(2, 2)	(2, 2)	0	1
		(1, 0)	(1, 0)	(2, 0)	0	1
				(1, 1)	0	1
			(1, 1)	(2, 1)	0	1
			(2, 0)	(2, 1)	0	1
			(2, 1)	(0, 0)	1	1
				(1, 1)	0	1
		(1, 0)	(2, 1)	(2, 2)	0	1
			(2, 2)	(1, 0)	1	1
		(1, 1)	(1, 1)	(2, 2)	0	1
			(2, 0)	(0, 0)	1	1
			(2, 1)	(1, 0)	1	1
			(2, 2)	(2, 0)	1	1
		(2, 0)	(2, 0)	(2, 2)	0	1
			(2, 1)	(1, 0)	1	1
			(2, 2)	(1, 1)	1	1
		(2, 1)	(2, 1)	(2, 0)	1	1
			(2, 1)	(1, 1)	1	1
			(2, 2)	(2, 1)	1	1
		(2, 2)	(2, 2)	(0, 0)	2	1
3	1	(0, 0, 0)	(0, 0, 0)	(0, 0, 0)	0	1
			(1, 0, 0)	(1, 0, 0)	0	1
			(1, 1, 0)	(1, 1, 0)	0	1
			(1, 1, 1)	(1, 1, 1)	0	1
		(1, 0, 0)	(1, 0, 0)	(1, 1, 0)	0	1
			(1, 1, 0)	(1, 1, 1)	0	1
			(1, 1, 1)	(0, 0, 0)	1	1
		(1, 1, 0)	(1, 1, 0)	(0, 0, 0)	1	1
			(1, 1, 1)	(1, 0, 0)	1	1
		(1, 1, 1)	(1, 1, 1)	(1, 1, 0)	1	1

FIG. 10. Structure constants in $qH^*\mathrm{Gr}(r,k)$ for $r+k=4$. Note $N_{ab}^{c,d}(r,k) = N_{ba}^{c,d}(r,k)$.

Appendix B: Leaky entanglers

There is also a differential-geometric proof that $\mathrm{LogSpec}\,\gamma(P_{\mathrm{CZ}}^2)$ has vanishing volume which does not rely on first knowing the precise region. The gate CZ commutes with Z–rotations:

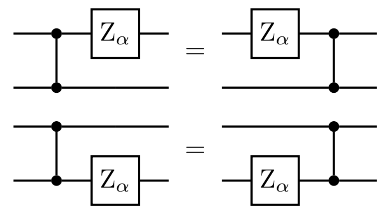

from which we may conclude the following for a generic pair of local one-qubit gates K_1 and K_2:

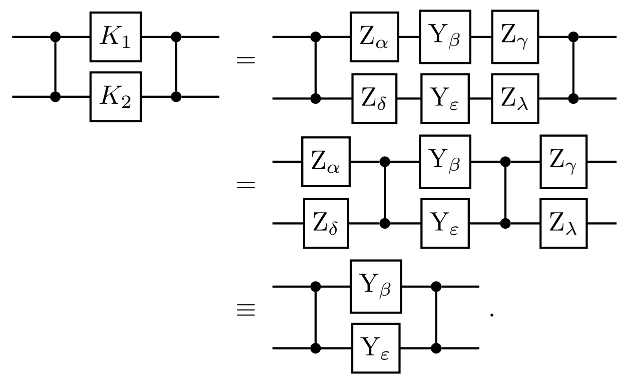

This circuit therefore traces out at most a two-parameter subfamily of gates within the fundamental alcove, which cannot be the image of a top dimensional set in $PU(4)$ and hence cannot have positive Haar volume.

This kind of argument turns out to be flexible enough that the commutation property powering it deserves its own name:

Definition 62. A two-qubit gate U is said to *leak (on the first qubit wire)* when there are exponential families A_θ, B_θ, and C_θ such that

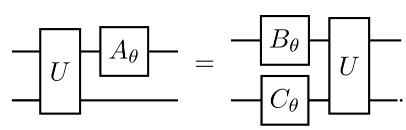

In fact, the other two-qubit gates in the Quil standard library are also leaky, as portrayed in Figure 11. This table has two remarkable features: first, that there are so many such relations, and second, that the single-qubit rotation is always a Z. We now show that at least the second of these is to be expected:

Lemma 63. *Leakiness is invariant under $\equiv_L$. Specifically, if U satisfies*

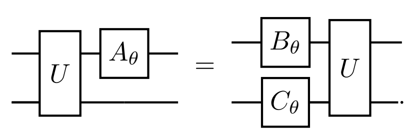

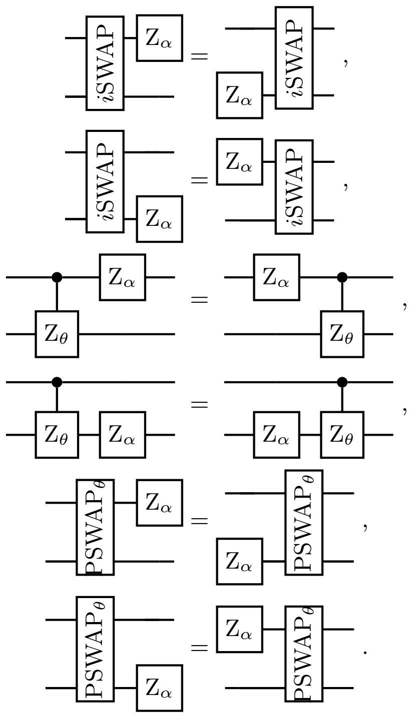

FIG. 11. Leakiness relations for the standard Quil gates

for some single-qubit exponential families A, B, C, and if V is given by

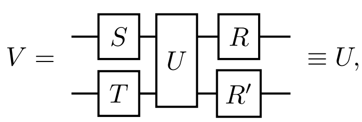

then we also have

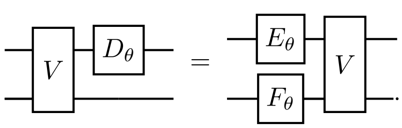

for $D_\theta = A_\theta^R$, $E_\theta = B_\theta^S$, and $F_\theta = C_\theta^T$.

Proof. This is a direct calculation:

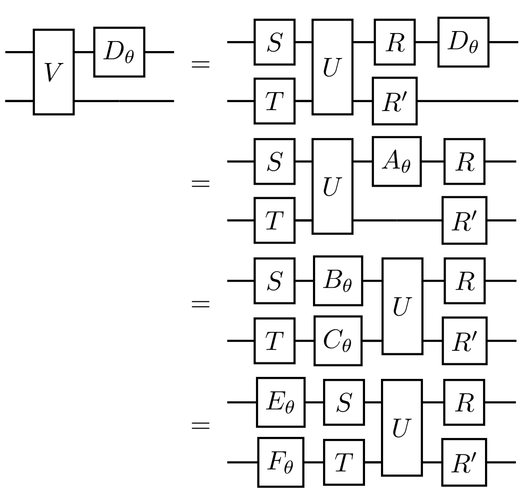

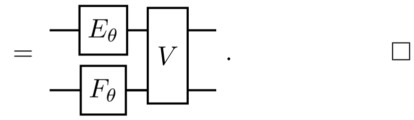

Remark 64. Suppose U is as in Lemma 63. By picking single-qubit operators R, S, and T with

$$A_{k\theta}^R = \mathrm{Z}_\theta, \qquad B_{k\theta}^S = \mathrm{Z}_{\ell\theta}, \qquad C_{k\theta}^T = \mathrm{Z}_{\ell'\theta},$$

we may replace U by V, also as in Lemma 63, for which we then have

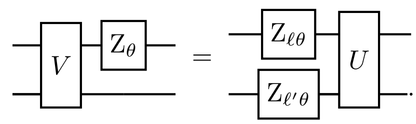

In fact, if U has a second leakiness relation on the other qubit wire, transforming the single-qubit gate A'_θ into the local operator $B'_\theta \otimes C'_\theta$, one may reuse S and T: because $A \otimes 1$ and $1 \otimes A'$ commute, $B \otimes C$ and $B' \otimes C'$ must also commute, which forces B and B' (hence B^S and $(B')^S$) to lie in the same one-parameter family and the same for C and C' (hence C^T and $(C')^T$).

However, the first observation—that Smith, Curtis, and Zeng's standard library contains so many leaky gates—is much more of an accident.

Lemma 65. *A generic entangler does not leak.*

Proof. At the level of Lie algebras, a leaky gate U satisfies

$$\mathrm{Ad}_U(\mathfrak{su}(2) \oplus 0) \cap (\mathfrak{su}(2) \oplus \mathfrak{su}(2)) \neq \emptyset,$$

witnessed by anti-Hermitian matrices

$$h = \begin{pmatrix} c & a + bi \\ -a + bi & d \end{pmatrix},$$

and

$$h' \otimes h'' = \begin{pmatrix} (c_0 + c_1)i & a_0 + b_0 i & a_0 + b_1 i & 0 \\ -a_0 + b_0 i & (-c_0 + c_1)i & 0 & a_1 + b_1 i \\ -a_1 + b_1 i & 0 & (c_0 - c_1)i & a_0 + b_0 i \\ 0 & -a_1 + b_1 i & -a_0 + b_0 i & -(c_0 + c_1)i \end{pmatrix}$$

which in particular satisfy

$$U^{-1} \left(\begin{array}{c|c} h & 0 \\ \hline 0 & h \end{array} \right) U = h' \otimes h''.$$

Elements of this product are computed by

$$(h' \otimes h'')_{i\ell} = \sum_{p=0}^{1} \sum_{j,k=1}^{2} \overline{U_{(2p+j)i}} h_{(2p+j)(2p+k)} U_{(2p+k)\ell},$$

which for a fixed value of U gives a linear system of *real* equations in the *real* unknowns specifying the elements of $\mathfrak{su}(2) \otimes 1$ and $\mathfrak{su}(2) \otimes \mathfrak{su}(2)$.

We claim that this system is generically of full rank, i.e., there is no solution but the trivial one. This system drops rank only when all determinants of all maximal subminors of the system vanish. As each determinant is an algebraic function on the real algebraic variety determined by $SU(4)$, if these do not all simultaneously vanish everywhere, then they generically do not simultaneously vanish. We therefore need only exhibit a point where the system has full rank for the conclusion to follow. Selecting $g = \sqrt{i\text{SWAP}}$, we make the manual calculation that the above system of equations is satisfied only for $h = 0$, $h' = h'' = 0$. □

Remark 66. The above mode of proof can be adapted to show that a generic entangler U has associated set P_U^2 of positive volume. For a variable choice of entangler U, we define an algebraic function

$$\begin{aligned} \text{cov}\colon\ SU(4) \times (SU(2)^{\otimes 2})^{\times 3} &\to SU(4) \\ (U, A, B, C) &\mapsto AU^{-1}BUC. \end{aligned}$$

Fixing a value of U and reassociating, this describes a function

$$\begin{aligned} \text{cov}_U\colon\ (SU(2)^{\otimes 2})^{\times 3} &\to SU(4) \\ (A, B, C) &\mapsto AU^{-1}BUC. \end{aligned}$$

The image of any smooth map, including cov_U, has positive volume if and only if there is a point in the domain at which the map has full rank. In turn, if an algebraic map, such as the unrestricted function cov, has full rank at any point, then it has full rank almost everywhere. Selecting U to be the B–gate [3], it is known that cov_B is surjective, hence its image has positive volume, hence there is a point $x = (A, B, C)$ at which cov_B has full rank.

That cov_B is of full rank is detected by the the condition that not all 15×15 minor determinants of $T_x\text{cov}_B$ of simultaneously vanish for some choice of $x = (A, B, C)$. Instead fixing such an x and considering these determinants as a family of *algebraic* functions of $U \in SU(4)$, we have thus seen that they are not all simultaneously vanishing for the particular point $B \in SU(4)$. It is then a consequence of the real Zariski topology that these functions are not simultaneously vanishing for a generic choice of $U \in SU(4)$.

Remark 67. On the other hand, leakiness is an essential part of quantum error correction codes: the very definition of a nonleaky multi-qubit gate means that a locally correctable error becomes a locally uncorrectable error after application of the entangler. This completely inhibits stabilizer-type codes from functioning.

[1] V. V. Shende, S. S. Bullock, and I. L. Markov, Physical Review A **70**, 012310 (2004), arXiv:quant-ph/0308045 [quant-ph].

[2] B. Kraus and J. I. Cirac, Physical Review A **63**, 062309 (2001), arXiv:quant-ph/0011050 [quant-ph].

[3] J. Zhang, J. Vala, S. Sastry, and K. B. Whaley, Phys. Rev. Lett. **93**, 020502 (2004), arXiv:quant-ph/0312193 [quant-ph].

[4] J. Zhang, J. Vala, S. Sastry, and K. B. Whaley, Phys. Rev. A **67**, 042313 (2003).

[5] V. V. Shende, I. L. Markov, and S. S. Bullock, Phys. Rev. A **69**, 062321 (2004).

[6] S. A. Caldwell, N. Didier, C. A. Ryan, E. A. Sete, A. Hudson, P. Karalekas, R. Manenti, M. P. da Silva, R. Sinclair, E. Acala, N. Alidoust, J. Angeles, A. Bestwick, M. Block, B. Bloom, A. Bradley, C. Bui, L. Capelluto, R. Chilcott, J. Cordova, G. Crossman, M. Curtis, S. Deshpande, T. E. Bouayadi, D. Girshovich, S. Hong, K. Kuang, M. Lenihan, T. Manning, A. Marchenkov, J. Marshall, R. Maydra, Y. Mohan, W. O'Brien, C. Osborn, J. Otterbach, A. Papageorge, J. P. Paquette, M. Pelstring, A. Polloreno, G. Prawiroatmodjo, V. Rawat, M. Reagor, R. Renzas, N. Rubin, D. Russell, M. Rust, D. Scarabelli, M. Scheer, M. Selvanayagam, R. Smith, A. Staley, M. Suska, N. Tezak, D. C. Thompson, T. W. To, M. Vahidpour, N. Vodrahalli, T. Whyland, K. Yadav, W. Zeng, and C. Rigetti, Physical Review Applied **10**, 034050 (2018), arXiv:1706.06562 [quant-ph].

[7] N. Schuch and J. Siewert, Physical Review A **67**, 032301 (2003), arXiv:quant-ph/0209035 [quant-ph].

[8] *Novi commentarii Academiae Scientiarum Imperialis Petropolitanae*, Vol. t.20 (1775) (Petropolis, Typis Academiae Scientarum,, 1775) p. 776.

[9] Y. Makhlin, Quantum Information Processing **1**, 243 (2002).

[10] E. Falbel and R. A. Wentworth, Topology **45**, 65 (2006).

[11] J. E. Humphreys, *Reflection groups and Coxeter groups*, Cambridge Studies in Advanced Mathematics, Vol. 29 (Cambridge University Press, Cambridge, 1990) pp. xii+204.

[12] R. S. Smith, M. J. Curtis, and W. J. Zeng, arXiv e-prints , arXiv:1608.03355 (2016), arXiv:1608.03355 [quant-ph].

[13] J. Lawrence, Math. Comp. **57**, 259 (1991).

[14] A. W. Cross, L. S. Bishop, S. Sheldon, P. D. Nation, and J. M. Gambetta, arXiv e-prints , arXiv:1811.12926 (2018), arXiv:1811.12926 [quant-ph].

[15] M. A. Nielsen, Physics Letters A **303**, 249 (2002).

[16] L. H. Pedersen, N. M. Møller, and K. Mølmer, Phys. Lett. A **367**, 47 (2007), arXiv:quant-ph/0701138 [quant-ph].

[17] P. Watts, J. Vala, M. M. Müller, T. Calarco, K. B. Whaley, D. M. Reich, M. H. Goerz, and C. P. Koch, Phys. Rev. A **91**, 062306 (2015).

[18] A. Edelman, T. A. Arias, and S. T. Smith, SIAM J. Matrix Anal. Appl. **20**, 303 (1999).

[19] J. Rå de, J. Reine Angew. Math. **431**, 123 (1992).

[20] C. Franks, arXiv e-prints , arXiv:1801.01412 (2018), arXiv:1801.01412 [math.CO].

[21] P. Bürgisser, C. Franks, A. Garg, R. Oliveira, M. Walter, and A. Wigderson, arXiv e-prints , arXiv:1804.04739 (2018), arXiv:1804.04739 [cs.DS].

[22] A. Horn, Pacific J. Math. **12**, 225 (1962).

[23] A. A. Klyachko, Selecta Math. (N.S.) **4**, 419 (1998).
[24] A. Knutson, arXiv Mathematics e-prints , math/9911088 (1999), arXiv:math/9911088 [math.RA].
[25] M. F. Atiyah, Bull. London Math. Soc. **14**, 1 (1982).
[26] V. Guillemin and S. Sternberg, Invent. Math. **67**, 491 (1982).
[27] V. Guillemin and S. Sternberg, Invent. Math. **77**, 533 (1984).
[28] F. Kirwan, Invent. Math. **77**, 547 (1984).
[29] E. Meinrenken and C. Woodward, eprint arXiv:dg-ga/961201 , dg-ga/9612018 (1996), arXiv:dg-ga/9612018 [math.DG].
[30] M. F. Atiyah and R. Bott, Philos. Trans. Roy. Soc. London Ser. A **308**, 523 (1983).
[31] S. K. Donaldson, J. Geom. Phys. **8**, 89 (1992).
[32] E. Meinrenken and C. Woodward, J. Differential Geom. **50**, 417 (1998).
[33] M. S. Narasimhan and C. S. Seshadri, Ann. of Math. (2) **82**, 540 (1965).
[34] S. K. Donaldson, J. Differential Geom. **18**, 269 (1983).
[35] V. B. Mehta and C. S. Seshadri, Math. Ann. **248**, 205 (1980).
[36] S. Agnihotri and C. Woodward, Math. Res. Lett. **5**, 817 (1998).
[37] W. Fulton and R. Pandharipande, in *Algebraic geometry—Santa Cruz 1995*, Proc. Sympos. Pure Math., Vol. 62 (Amer. Math. Soc., Providence, RI, 1997) pp. 45–96.
[38] M. Kontsevich and Y. Manin, Comm. Math. Phys. **164**, 525 (1994).
[39] A. Bertram, I. Ciocan-Fontanine, and W. Fulton, J. Algebra **219**, 728 (1999).
[40] A. Buch, "Littlewood–Richardson calculator," `http://sites.math.rutgers.edu/~asbuch/lrcalc/` (1999-2014).
[41] P. Belkale, Compositio Math. **129**, 67 (2001).